

1 Cytotoxic CD4⁺ T cells in the bone marrow compromise healthy ageing 2 by enhancing granulopoiesis

3

4 Enrique Gabandé-Rodríguez ^{1, #,*}, Gonzalo Soto-Heredero ^{1,2, #}, Elisa Carrasco ^{1,3,4,5},
5 Carlos Anerillas ⁶, José Ignacio Escrig-Larena ^{1,2}, Sandra Delgado-Pulido ^{1,2}, Isaac
6 Francos-Quijorna ^{1,2,4}, Manuel M. Gómez de las Heras ^{1,2}, Álvaro Fernández-Almeida ¹,
7 Eva María Blanco ¹, Elia Winand-Osete ¹, Virginia Zorita ⁷, Jorge Martínez-Cano ⁸,
8 Amanda Garrido ⁹, Rafael de Cabo ⁹, Santos Mañes ¹⁰, Myriam Gorospe ⁶
9 and María Mittelbrunn ^{1,*}.

10

11 ¹ Tissue and Organ Homeostasis Program, Cell-cell communication and inflammation
12 Unit, Centro de Biología Molecular Severo Ochoa (CBMSO), Consejo Superior de
13 Investigaciones Científicas (CSIC), Madrid, Spain.

14 ² Department of Molecular Biology, Faculty of Sciences, Universidad Autónoma de
15 Madrid (UAM), Madrid, Spain.

16 ³ Department of Biology, Faculty of Sciences, Universidad Autónoma de Madrid,
17 Madrid, Spain.

18 ⁴ Instituto Universitario de Biología Molecular-IUBM (Universidad Autónoma de
19 Madrid), Madrid, Spain.

20 ⁵ Instituto Ramón y Cajal de Investigación Sanitaria (IRYCIS), Madrid, España

21 ⁶ Laboratory of Genetics and Genomics, National Institute on Ageing Intramural
22 Research Program, National Institutes of Health, Baltimore, MD, USA.

23 ⁷ Centro Nacional de Investigaciones Cardiovasculares (CNIC), Madrid, Spain.

24 ⁸ Interactions with the environment Program, Immune system development and
25 function Unit, Centro de Biología Molecular Severo Ochoa (Consejo Superior de
26 Investigaciones Científicas -Universidad Autónoma de Madrid), Madrid, Spain.

27 ⁹ Translational Gerontology Branch, National Institute on Ageing Intramural Research
28 Program, National Institutes of Health, Baltimore, MD, USA.

29 ¹⁰ Department of Immunology and Oncology, Centro Nacional de Biotecnología,
30 Consejo Superior de Investigaciones Científicas (CSIC), 28049 Madrid, Spain.

31 [#] These authors contributed equally to this work

32 ^{*} Correspondence to: mmittelbrunn@cbm.csic.es, egabande@cbm.csic.es

33 Abstract

34 Neutrophils are the most abundant leukocytes in the blood, with numbers further
35 increasing with age. Despite their essential role as a primary line of defense, neutrophils
36 can contribute to tissue damage and age-related diseases ¹ and a high neutrophil-to-
37 lymphocyte ratio predicts all causes of mortality in the elderly ²⁻⁵. However, the precise
38 mechanisms driving enhanced neutrophil generation during ageing remain poorly
39 understood. Here, we show that a subset of CD4⁺ T cells with a cytotoxic phenotype
40 (CD4⁺ CTLs) producing the chemokine CCL5 and harbouring dysfunctional
41 mitochondria, infiltrate the bone marrow and induce granulopoiesis in aged mice. During
42 ageing, hematopoietic stem cells upregulate CCR5, the primary receptor for CCL5, and
43 its deficiency limits the T cell-mediated induction of granulopoiesis and neutrophil
44 output. Treatment with the FDA-approved CCR5 inhibitor Maraviroc decreases
45 granulopoiesis and lowers the levels of circulatory and tissue-infiltrating neutrophils,
46 ameliorating multiple ageing biomarkers and improving functional outcomes in aged
47 mice. These findings suggest that age-associated alterations in T cells reduce health
48 outcomes by remodelling the bone marrow niche and enhancing neutrophil generation.
49 Consequently, interventions to disrupt the interplay between T cells and hematopoietic
50 stem cells hold substantial therapeutic potential to ameliorate age-associated diseases.

51

52

53 **Key words:** T cells, neutrophils, granulopoiesis, CCL5, CCR5, Maraviroc, CD4⁺ CTL

54

55

56

57

58

59

60 Main

61 During ageing, impaired immune cell function increases the risk of suffering cancer and
62 infections. Additionally, faulty immune cells sustain inflammageing ⁶, a persistent
63 chronic inflammation that exacerbates several age-associated pathologies including
64 cardiovascular disease, diabetes, chronic kidney disease, non-alcoholic fatty liver disease,
65 autoimmune and neurodegenerative disorders, jointly representing the leading causes of
66 disability and mortality worldwide ^{7,8}.

67 Despite their relatively short lifespan, neutrophils are the most abundant
68 leukocytes in the blood. Upon encountering danger signals, neutrophils rapidly migrate
69 to target tissues to efficiently eliminate pathogens employing various mechanisms such
70 as phagocytosis, degranulation, or suicide to release DNA in neutrophil extracellular
71 traps. However, increased numbers of hyper-responsive neutrophils may contribute to
72 tissue damage during ageing ⁹. For example, neutrophils engaged in reverse
73 transendothelial migration re-enter the circulation from inflamed aged tissues and
74 disseminate to the lungs, causing vascular leakage and remote damage ¹⁰. Moreover,
75 tissue-infiltrating neutrophils have the capacity to induce paracrine senescence by
76 triggering telomere damage through the release of reactive oxygen species ¹¹.

77 The number of circulating neutrophils increases with age, in part due to the
78 skewing of haematopoiesis towards the production of myeloid precursors at the expense
79 of lymphoid progenitors ¹². This imbalanced differentiation ultimately results in an
80 increased neutrophil-to-lymphocyte ratio (NLR) in the circulation. Remarkably, a high
81 NLR serves as a strong predictor of mortality in virtually all age-associated diseases ²⁻⁵.
82 Therefore, understanding the mechanisms driving enhanced granulopoiesis and a
83 heightened NLR during ageing may critically change the way multiple age-associated
84 diseases are managed.

85 Recent reports indicate that T cells infiltrate the bone marrow (BM) and eventually
86 lead to increased granulopoiesis and circulatory neutrophils under acute psychological
87 stress, prolonged starvation, or autoimmune disease¹³⁻¹⁶. Here, we report that ageing is
88 associated with increased numbers of CD4⁺ CTLs in the BM. By paracrine signalling to
89 adjacent aged hematopoietic stem cells (HSCs), CD4⁺ CTLs induce granulopoiesis, rising
90 the levels of peripheral neutrophils and augmenting the NLR through a targetable
91 CCL5/CCR5 axis, ultimately contributing to inflammageing and tissue senescence.

92 **Results**

93

94 **Accumulation of CD4⁺ T cells in the bone marrow enhances granulopoiesis and**
95 **increases CXCR4^{hi} CD62L^{lo} neutrophils in old mice**

96 To understand how ageing influences the generation and fate of neutrophils, we
97 performed multiparametric spectral flow cytometry to analyse the percentage of the
98 different blood populations in old (24 months old) versus young (3 months old) mice.
99 Uniform manifold approximation and projection (UMAP) representation showed
100 increased numbers of circulating neutrophils and monocytes together with reduced
101 circulating lymphocyte numbers (Fig. 1a and Extended Data Fig. 1a,b), resulting in an
102 increased NLR (Fig. 1b). Of note, we observed a higher percentage of pro-inflammatory
103 circulating CXCR4^{hi}CD62L^{lo} neutrophils and a decreased percentage of
104 CXCR4^{lo}CD62L^{hi} naïve neutrophils^{17,18} in old mice (Fig. 1c). Compared with
105 CXCR4^{lo}CD62L^{hi} neutrophils, CXCR4^{hi}CD62L^{lo} neutrophils displayed a pro-
106 inflammatory profile characterized by the upregulation of ICAM-1, TLR-4, CD11b,
107 CD66a or CD101 and the downregulation of CXCR2 (Extended Data Fig. 1c). The
108 increased numbers of circulating CXCR4^{hi}CD62L^{lo} neutrophils correlated with an
109 increased presence of neutrophils exhibiting a pro-inflammatory phenotype in the spleen
110 (Extended Data Fig. 1d), and increased infiltration in the kidney, lung and liver in old
111 mice compared with young mice (Extended Data Fig. 1e,f). To study whether these
112 changes in the phenotype of neutrophils occurred by exposure to an aged environment,
113 we performed heterochronic adoptive transfer experiments of peripheral blood leukocytes
114 from young mice (CD45.1) to either young or old recipient mice (CD45.2). Four hours
115 later, we analysed the phenotype of the transferred CD45.1 neutrophils in the blood (Fig.
116 1d). Transferred neutrophils acquired a CXCR4^{hi}CD62L^{lo} profile more rapidly in old than
117 in young recipients (Fig. 1e,f), supporting a cell-extrinsic induction of this phenotype.

118 According to previous data, this rise in neutrophils correlated with a skewing of
119 haematopoiesis during ageing (Fig. 1g and Extended Data Fig. 2). Aged mice exhibited
120 increased percentages of haematopoietic stem cells (HSCs) and granulocyte-monocyte
121 precursors (GMPs) (Fig. 1g), together with increased numbers of neutrophils and
122 monocytes in the BM (Extended Data Fig. 1g).

123 As recent evidence supports the notion that T cells infiltrate the BM and influence
124 haematopoiesis during stressful and autoimmune conditions ¹³⁻¹⁶, we wondered whether
125 this mechanism also operates in old mice. We observed that, unlike in the blood, lymph
126 nodes and spleen, old mice exhibited an increased percentage of CD4⁺ T cells in the BM
127 (Fig. 1h and Extended Data Fig. 3a-c). To directly dissect the capacity of aged CD4⁺ T
128 cells to induce granulopoiesis, we performed adoptive transfer experiments of CD4⁺ T
129 cells from young and old mice into T- and B-cell-deficient recipient (*Rag1*^{-/-}) mice ¹⁹ and
130 we analysed the frequency of BM hematopoietic precursors 7 days post-transfer (Fig. 1i).
131 Compared with the transfer of CD4⁺ T cells from young mice, infusion of CD4⁺ T cells
132 from old mice led to enhanced frequencies of LS⁺K cells and downstream granulocyte-
133 monocyte progenitors (GMPs) together with an increased frequency of BM neutrophils
134 (Fig. 1j), indicating that old CD4⁺ T cells promote granulopoiesis. Further supporting a
135 role of T cells in the regulation of myeloid cell generation, old *Cd3e*^{-/-} mice lacking T
136 cells exhibited lower levels of circulating neutrophils and monocytes than age-matched
137 control mice (Extended Data Fig. 1h).

138 Altogether, these results indicate that T cells accumulate in the BM during ageing
139 leading to enhanced granulopoiesis and neutrophil output.

140 **CCL5⁺ CD4⁺ CTLs accumulate in the bone marrow during ageing**

141 Single-cell analyses have uncovered the heterogeneity of T cells during ageing in
142 different organs such as the spleen, peritoneum, lung and liver ^{20,21}. Based on these
143 observations, we implemented a panel of 15 antibodies that allows to explore the diversity
144 of CD4⁺ T cells in the BM during ageing by spectral flow cytometry (Fig. 2a,b and
145 Extended Data Fig. 4). Unbiased analysis of CD4⁺ T cells from the BM by UMAP and
146 ulterior clusterization identified 9 clusters, including naïve T cells (cluster 1 or “Naïve”),
147 resting and activated T regulatory cells (clusters 2 and 3 or “rTregs” and “aTregs”,
148 respectively). Among the rest of the clusters, we identified T central memory T cells
149 (cluster 4 or “TCM”), effector memory T cells (cluster 5 or “TEM”), PD-1⁺ T cells
150 (cluster 6 or “PD-1⁺”), a cluster defined by the co-expression of CXCR6 and CD38
151 (cluster 7 or “CXCR6⁺”), a CCL5⁺ cluster (cluster 8 or “CCL5⁺”) and a cluster lacking
152 expression of most of the assessed markers (cluster 9) (Fig. 2a,b and Extended Data Fig.
153 4). We compared the proportion of all subsets in old versus young mice (Fig. 2c). As
154 expected, the two naïve subsets (clusters 1 and 2) were significantly enriched in young
155 mice and the aTregs cluster showed a similar abundance in both groups of age. Notably,

156 the TCM, TEM and CXCR6⁺ clusters were enlarged in young mice. Conversely, T cells
157 included in the PD-1⁺ cluster increased in old mice. Critically, the vast majority of BM
158 CD4⁺ T cells showing a significant accumulation in old mice grouped in the CCL5⁺
159 cluster, accounting for >25% of the CD4⁺ cells while it was negligible in young mice
160 [CCL5⁺: mean young/old: 1.64/26.78, p < 0.0001] (Fig. 2c). The CCL5⁺ cluster was
161 characterized by expressing high levels of the activation marker CD38, the transcription
162 factor Eomesodermin (EOMES) and the checkpoint inhibitor PD-1 together with a low
163 expression of CD44 (Fig. 2b and Extended Data Fig. 4), resembling cytotoxic T cells
164 (CD4⁺ CTLs)²⁰. Positive expression of Perforin in most BM CD4⁺ CCL5⁺ cells from old
165 mice further confirmed the cytotoxic identity of this cluster (Fig. 2d).

166 **Bone marrow CD4⁺ CTLs harbour depolarized mitochondria**

167 T cell ageing correlates with a mitochondrial function decline^{22,23}. We tested whether
168 CD4⁺ CTLs in old mice exhibit mitochondrial dysfunction by using the Mitotracker
169 Green probe (MtG), which stains the whole mitochondrial mass pool, in combination with
170 Mitotracker Deep Red (MtDR), whose incorporation depends on the mitochondrial
171 membrane potential. This technique permits the identification of cells harbouring healthy
172 mitochondria (MtDR^{hi}MtG^{hi}) or depolarized mitochondria (MtDR^{lo}MtG^{lo}, and
173 MtDR^{lo}MtG^{hi}). Comparison of CD4⁺ T cells from the BM, spleen, and Peyer's patches
174 revealed that MtDR^{lo}MtG^{lo} and MtDR^{lo}MtG^{hi} CD4⁺ T cells more frequently accumulated
175 in the BM than in the rest of the tissues in old mice (Extended Data Fig. 5a-c), suggesting
176 that aged T cells with dysfunctional mitochondria preferentially accumulate in the BM.

177 To identify which of the T cell clusters harbour dysfunctional mitochondria, we
178 first performed analysis of publicly available scRNASeq databases applying Gene Set
179 Enrichment Analysis (GSEA) to compare significantly altered pathways between CD4⁺
180 CTLs and the rest of the CD4⁺ T cell subsets²⁰. This approach evidenced a
181 downregulation of several mitochondrial function-related pathways in the CD4⁺ CTL
182 cluster (Fig. 2e). Hence, we evaluated the mitochondrial membrane potential in the
183 different T cell subsets in the BM. To overcome the impossibility of fixing the MtG dye,
184 we set up a panel of antibodies against extracellular markers to identify the different
185 clusters of BM T cells (Extended Data Fig. 6a). CD4⁺ CTLs were identified as
186 CD44^{lo}CD62L⁻CD38^{hi} and intracellular staining for CCL5 confirmed that the majority of
187 CCL5⁺ cells were included in this population (Extended Data Fig. 6b and Supplementary
188 Table 1). With this strategy, we observed similar proportions of the different clusters in

189 the aged BM to that observed by unbiased clusterization, with a remarkable accumulation
190 of CD4⁺ CTLs (Extended Data Fig. 6b,c). Of note, cells identified as CD4⁺ CTL contained
191 the highest percentage of T cells with MtDR^{lo}MtG^{lo} and MtDR^{lo}MtG^{hi} depolarized
192 mitochondria (Fig. 2f,g and Supplementary Table 2) and therefore showed a
193 concomitantly decreased MtDR/MtG ratio (Extended Data Fig. 6d and Supplementary
194 Table 1). Taken together, these results support the notion that T cells with dysfunctional
195 mitochondria exhibiting a CD4⁺ CTL profile accumulate in the BM during ageing.

196 **Increased granulopoiesis in mice with mitochondrial dysfunction in T cells**

197 In light of the accumulation of depolarized mitochondria in CD4⁺ CTLs, we investigated
198 whether a deteriorated mitochondrial function in CD4⁺ T cells was sufficient to induce
199 CTL conversion and granulopoiesis skewing. To this end, we used mice with a T cell-
200 specific deletion of the mitochondrial transcription factor A (*Tfam*) gene by crossing
201 *Tfam*^{fl/fl} mice with mice expressing the CRE recombinase under the *Cd4* promoter
202 (CD4^{Cre}) (Extended Data Fig. 7a). T cells from CD4^{Cre} *Tfam*^{fl/fl} mice display an activated
203 phenotype^{6,24}, inducing the expression of inflammapoiesis-associated cytokines that
204 trigger paracrine senescence and age-associated multimorbidity⁶. At 8 months old,
205 CD4^{Cre} *Tfam*^{fl/fl} mice presented an accumulation of CD4⁺ CTLs similar to observed in 24
206 months old mice (Extended Data Fig. 7b, Fig. 2c). Analysis of circulating immune cell
207 populations showed a remarkable accumulation of neutrophils together with a decrease
208 of T and B cells (Extended Data Fig. 7c,d and Extended Fig. 2a) that correlated with a
209 concomitantly increased NLR (Extended Data Fig. 7e), mirroring observations in old
210 mice (Fig. 1a,b and Extended Fig. 1b). Supporting the idea that enhanced granulopoiesis
211 contributes to the increased levels of circulatory neutrophils, we detected an increased
212 percentage of GMPs in the BM of CD4^{Cre} *Tfam*^{fl/fl} mice (Extended Data Fig. 7f). CD4^{Cre}
213 *Tfam*^{fl/fl} mice also presented increased levels of circulating pro-inflammatory
214 CXCR4^{hi}CD62L^{lo} neutrophils (Extended Data Fig. 7g) and increased numbers of splenic
215 neutrophils and monocytes (Extended Data Fig. 7h) together with infiltrating
216 myeloperoxidase-positive (MPO) neutrophils in the kidney, liver and lung (Extended
217 Data Fig. 7i,j). Altogether, these findings suggest that mitochondrial dysfunction in T
218 cells promotes CD4⁺ CTL differentiation and granulopoiesis induction, mirroring
219 observations in naturally aged mice.

220 **Prolonged TCR stimulation in an aged milieu induces mitochondrial dysfunction
221 and CCL5⁺ CD4⁺ CTL differentiation.**

222 To investigate whether the differentiation of T cells towards CCL5⁺ CD4⁺ CTL is
223 triggered by exposure to an aged environment, we performed heterochronic adoptive
224 transfer of CD45.1 CD4⁺ T cells isolated from young mice into either young or old
225 CD45.2 recipient mice (Fig. 3a). Analysis of T cells 14 days post-transfer showed an
226 increased percentage of CD45.1⁺ CD4⁺ CTLs in the blood of old compared to young
227 recipient mice (Fig. 3b). By 21 days post-transfer, old mice presented ~ 60% of CD45.1⁺
228 BM T cells exhibiting a CD4⁺ CTL profile, contrasting with a ~ 3% in the BM of young
229 recipients (Fig. 3c). Additionally, ageing of the host correlated with an increased
230 infiltration of CD45.1 CD4⁺ CTLs in different tissues. Of note, comparison of the
231 percentage of CD45.1 CD4⁺ CTL in the BM, the liver, the white adipose tissue and the
232 colon, revealed that donor cells were particularly enriched in the BM during ageing, with
233 a remarkable 18.5-fold increase of young levels, confirming that the BM is a preferential
234 site for CD4⁺ CTL migration (Fig. 3d).

235 To assess if the conversion to CCL5⁺ CD4⁺ CTL in an aged environment was due
236 to chronic TCR stimulation or to exposure to inflammeing-associated cytokines, we
237 adoptively transferred CD4⁺ cells isolated from young CD45.1 and OT-II CD45.2 mice
238 into old CD45.1.2 recipients in a 1:1 ratio and we analysed the differential infiltration of
239 donor CD4⁺ cells to the BM 14 days later (Fig. 3e). CD4⁺ cells from OT-II mice are
240 genetically engineered to express a TCR that exclusively recognizes a specific peptide of
241 the chicken ovalbumin. In the absence of this peptide, OT-II CD4⁺ cells cannot engage
242 TCR-dependent activation while remaining susceptible to cytokine-mediated activation
243 ²⁵. We detected a decreased percentage of both CCL5⁺ and PD-1⁺ OT-II CD45.2 T cells
244 in the BM of recipient mice 14 days after the adoptive transfer (Fig. 3f,g), suggesting that
245 TCR signalling is required for CTL differentiation in an aged environment. Furthermore,
246 we compared CD4⁺ cells acutely and chronically (16 days) stimulated in culture with anti-
247 CD3/anti-CD28 (Fig. 3h) and we observed an increased expression of CCL5 (Fig. 3i,j),
248 together with CD38, PD-1 and EOMES (Extended Data Fig. 8a-c), in chronically relative
249 to acutely TCR-stimulated cells. Furthermore, we observed that continuous TCR
250 stimulation led to the accumulation of dysfunctional mitochondria (MtDR^{lo}MtG^{lo} and
251 MtDR^{lo}MtG^{hi}) in cultured CD4⁺ T cells (Fig. 3k). In sum, these results support the notion
252 that exposure to an aged environment induces the differentiation of CD4⁺ cells into CD4⁺
253 CTLs, requiring prolonged TCR stimulation.

254

255 **Bone Marrow CD4⁺ CTLs induce granulopoiesis by CCL5/CCR5 signalling**

256 Given that signalling through CCL5 and CCR5 has been involved in the induction
257 of myeloid skewing in mouse models of multiple sclerosis^{15,26}, we studied the
258 contribution of this pathway to T cell-induced granulopoiesis during ageing. Notably, we
259 initially observed that HSCs from old mice exhibit an upregulation of CCR5, the main
260 CCL5 receptor, leading to increased percentages of CCR5⁺ HSCs in the BM of old mice
261 (Fig. 4a). To explore the relevance of signalling through CCL5/CCR5 in T cell-induced
262 granulopoiesis during ageing, we generated mixed BM chimeric mice by injecting 50%
263 of CD45.1 CCR5^{+/+} and 50% of CD45.2 CCR5^{-/-} BM cells into irradiated CD45.1.2
264 recipients. Two months later, we adoptively transferred CD4⁺ cells isolated from aged
265 mice and studied the effect in HSCs and downstream precursors of both genotypes one
266 week later (Fig. 4b). Flow cytometry analysis revealed a decreased percentage of LS⁺K
267 cells and GMPs in CD45.2 CCR5^{-/-} cells (Fig. 4c and Extended Fig. 2) that correlated
268 with decreased proportions of CD45.2 CCR5^{-/-} neutrophils and Ly6C^{hi} monocytes in the
269 BM (Fig. 4d). We also confirmed reductions in the percentages of blood CD45.2 CCR5^{-/-}
270 neutrophils and Ly6C^{hi} monocytes (Fig. 4e). Supporting a selective effect on the
271 myeloid lineage, we did not find reductions in the levels of either BM CD45.2 CCR5^{-/-}
272 CD8⁺ cells (Fig. 4f) or blood CD45.2 CCR5^{-/-} CD8⁺ cells (Fig. 4g). In aggregate, these
273 findings suggest that CCR5 signalling in HSCs is involved in T cell-induced
274 granulopoiesis in aged mice.

275 **Inhibition of CCR5 reverts myeloid skewing, decreases the NLR and improves
276 health status in aged mice**

277 To investigate whether interfering with CCR5 signalling could prevent age-associated
278 changes in haematopoiesis, we treated old mice for one month with Maraviroc, an FDA-
279 approved CCR5 antagonist²⁷ (Fig. 5a). Treatment with Maraviroc decreased the
280 percentage of GMPs and LS⁺K cells while increased the frequencies of common lymphoid
281 progenitors (CLPs) in old mice (Fig. 5b and Extended Fig. 2), confirming a reversion of
282 the skewing of haematopoiesis. Notably, treatment with Maraviroc decreased the
283 percentage of circulating neutrophils (Fig. 5c) and increased the percentage of CD4⁺ and
284 CD8⁺ T cells (Fig. 5d), leading to a concomitant normalisation of the NLR (Fig. 5e) in
285 old mice. These results suggest that CCR5 inhibition turns haematopoiesis into a more
286 youthful state.

287 We next studied whether restoring haematopoiesis with Maraviroc improves
288 health outcomes in old mice. Old mice treated with Maraviroc exhibited reduced levels
289 of infiltrating neutrophils in lung and liver (Fig. 5f), which correlated with a decreased
290 presence of senescent cells, identified as p16⁺, in the liver (Fig. 5g). Furthermore,
291 Maraviroc lowered the levels in serum of multiple inflammmageing-associated cytokines
292 (Fig. 5h), non-fasting glucose (Fig. 5i), albumin (Fig. 5j), alanine aminotransferase (ALT)
293 and aspartate aminotransferase (AST) (Fig. 5k). Notably, this correlated with the
294 normalisation of different physiological parameters affected in old mice including
295 metabolic alterations such as the respiratory exchange ratio (Fig. 5l), the loss of muscle
296 strength (Fig. 5m) and the impaired locomotor coordination (Fig. 5n). Taken together,
297 these results suggest that CCR5 inhibition by Maraviroc normalises granulopoiesis,
298 leading to improved health outcomes in old mice.

299

300 **Discussion**

301 CD4 CTLs are emerging as age-associated T cells, as their numbers correlate with
302 ageing^{20,28}. However, their origin and contribution to ageing are still debated. Previous
303 findings reported the presence of these cells mainly in conditions characterized by
304 continuous TCR stimulation such as viral infections²⁹. We found that young T cells
305 exposed to an aged environment differentiate into CD4⁺ CTL, requiring prolonged TCR
306 activation. It is tempting to speculate that an altered repertoire of presented antigens could
307 be the origin of CD4⁺ CTL differentiation in an aged environment. Regarding their
308 function, CD4⁺ CTLs are responsible of eliminating senescent cells in the skin³⁰ and may
309 be involved in the control of tumour growth³¹. Despite these potentially beneficial
310 functions, a massive accumulation of CD4⁺ CTL in the BM during ageing, either due to
311 enhanced migration or to delayed clearance, would result in a detrimental increase in
312 granulopoiesis and neutrophilia.

313 A skewing of haematopoiesis towards the production of myeloid cells is an ageing
314 feature with a major impact on immune system function, tissue homeostasis and
315 healthspan. Even though a high NLR is associated with bad prognoses in most age-
316 associated diseases²⁻⁵, the mechanisms driving altered haematopoiesis during ageing
317 remain incompletely understood. Previous findings have established that remodelling of

318 the BM stroma induces the skewing of haematopoiesis in aged mice. Accordingly,
319 inflammation triggered by $\beta 2/\beta 3$ adrenergic receptors induces haematopoiesis
320 skewing^{12,32}, at least in part, by increasing IL-1 β levels in aged mice³³. Similarly,
321 decreased levels of trophic factors such as IGF-1³⁴ or an altered cellular composition of
322 the BM niche, including a Notch-dependent reduction of blood vessels³⁵ or an
323 accumulation of adipocytes³⁶, alter the fate of haematopoietic precursors. Our findings
324 suggest that infiltration of CD4 $^+$ CTLs into the BM during ageing will be a critical factor
325 contributing to the remodelling of the BM niche. These cells, characterized by the
326 overexpression of CCL5, induce granulopoiesis by signalling to CCR5 in haematopoietic
327 precursors. These observations are in line with previous findings reporting enhanced
328 granulopoiesis and neutrophil generation by BM infiltrating autoreactive T cells in
329 multiple sclerosis¹⁵.

330 We found enhanced granulopoiesis resulting in elevated pro-inflammatory
331 CXCR4 $^{\text{hi}}$ CD62L $^{\text{lo}}$ neutrophils in old mice. Remarkably, recent evidence suggest that pro-
332 inflammatory neutrophils can induce paracrine senescence¹¹, trigger age-related lung
333 damage¹⁰, worsen myocardial infarction³⁷ and foster skin inflammation³⁸. Importantly,
334 we found that enhanced granulopoiesis in aged mice is prevented by pharmacological
335 inhibition of CCR5, correlating with an improvement of multiple ageing-associated
336 conditions. Supporting these findings, human individuals carrying homozygous loss of
337 function mutations in CCR5 (CCR5-Delta32) present better outcomes after stroke³⁹ and
338 during multiple sclerosis²⁶. Future studies should investigate whether this improvement
339 is mediated by a decreased induction of granulopoiesis, which contributes to aggravating
340 stroke and autoimmune neuroinflammation in mice^{15,40}.

341 In all, these findings place T cells as inducers of the disbalance in haematopoiesis
342 seen during ageing. As a high NLR is a predictor of mortality in most age-related
343 diseases²⁻⁵, and Maraviroc is already an FDA-approved drug for the treatment of HIV
344 patients²⁷, our results may have broad therapeutic implications for the treatment of age-
345 related pathologies. These findings set the stage for the development of drugs to eliminate
346 CD4 $^+$ CTLs, avoid their recruitment into the BM, and modify their interplay with
347 haematopoietic precursors to improve age-associated outcomes.

348 Acknowledgements

349 The authors thank María Navarro and César Cobaleda for critical discussion of the
350 manuscript. Research in the Mittelbrunn lab was supported by European Research
351 Council (ERC-2021-CoG 101044248-Let T Be), by Comunidad de Madrid (Spain)
352 (Y2020/BIO-6350 NutriSION-CM synergy) and by Spanish Ministerio de Ciencia e
353 Innovación (PID2022-141169OB-I00) grants. G.S-H. was supported by an FPI-UAM
354 grant from the Universidad Autónoma de Madrid and by Let T Be. E.G-R and I.F-Q were
355 supported by a Juan de la Cierva-Incorporación grant (IJC2018-036850-I and JC2020-
356 044392, respectively) from the Ministerio de Ciencia, Innovación y Universidades
357 (Spain) and by ERC-2021-CoG 101044248-Let T Be. M.M.G.H. and J.I.E.-L. were
358 supported by FPU grants (FPU19/02576 and FPU20/04066, respectively), both from
359 Ministerio de Ciencia, Innovación y Universidades (Spain). C.A., A.G., R.dC., and M.G.
360 are supported by the NIA IRP, NIH. We thank the Mouse Metabolism & Phenotyping
361 core in Baylor College of Medicine at Houston, Texas (USA) for analysis of serum
362 samples and the flow cytometry facility of CBMSO.

363 Methods

364 Animal procedures

365 All mice were bred and aged in the specific-pathogen-free facility of Centro de Biología
366 Molecular Severo Ochoa (CBMSO, Madrid, Spain) in accordance with European Union
367 recommendations and institutional guidelines. C57BL/6J HccRsd mice were purchased
368 from Envigo or bred at the CBMSO animal facilities. *Tfam*^{fl/fl} mice were kindly provided
369 by N.G. Larsson⁴¹, and CD4^{Cre+/wt} mice were purchased from the Jackson Laboratory.
370 Double heterozygotes (*Tfam*^{+/fl}, CD4^{Cre+/wt}) were obtained and backcrossed to
371 the *Tfam*^{fl/fl} strain to generate cell-specific knockouts (CD4^{Cre} *Tfam*^{fl/fl}). OT-II mice were
372 kindly provided by Dr. N. Martínez-Martín (CBMSO). CCR5^{-/-} mice were provided by
373 Prof. S. Mañes (CNB). *Rag1*^{-/-} (1547488)¹⁹, C57BL/6J CD45.1.2 and C57BL/6J CD45.1
374 mice were provided by Dr. C. Cobaleda (CBMSO). Surgical and experimental procedures
375 were approved by the ethics committee of the Consejo Superior de Investigaciones
376 Científicas (CSIC). Both male and female mice were used in this study. In general, mice
377 were used at different ages: young (less than 4 mo), old (22-25 mo) unless otherwise
378 specified in the figure legend.

379 *Adoptive transfer of immune cells*

380 For neutrophil analysis, whole blood from four donor C57BL/6 CD45.1 mice, previously
381 euthanized by exposure to CO₂, was isolated by cardiac puncture. Red blood cells were
382 removed in erythrocyte lysis buffer for 7 min and immune cells were resuspended in 0.9%
383 NaCl. Equal amounts of immune cells were i.v. injected into young or old CD45.2
384 recipients. The percentage of CXCR4^{hi}CD62L^{lo} and CXCR4^{lo}CD62L^{hi} was analyzed in
385 Ly6C⁺ Ly6G⁺ neutrophils before and four hours after the adoptive transfer.

386 For the adoptive transfer of CD4⁺ cells, the spleen and the axillary, mesenteric and
387 inguinal lymph nodes were harvested from either young and old C57BL/6 CD45.1,
388 C57BL/6 CD45.2 or OT-II (CD45.2) donor mice as specified in figures. Organs were
389 mashed and filtered through a 70-μm cell strainer and erythrocytes were removed in
390 erythrocyte lysis buffer for 5 min. CD4⁺ cells were purified with the MojoSort™ mouse
391 CD4 T cell isolation kit (Biolegend, 480006) according to manufacturer instructions.
392 CD4⁺ cells were resuspended in 0.9% NaCl and 6 million cells were i.v. injected into
393 every young and old C57BL/6 CD45.1, CD45.2 or CD45.1.2 recipient as specified in the
394 figure legends. The purity of CD4⁺ isolated cells was routinely tested by flow cytometry,
395 typically ranging from 85-95% of total cells.

396 *BM transplantation*

397 For BM transplantation, recipient mice were lethally irradiated with two doses of 5.5 Gy
398 and intravenously injected with 5 x 10⁶ cells. Mice were administered with 1 mg/ml of
399 neomycin in the drinking water for four weeks starting one week before transplantation.
400 Recipient mice were allowed to reconstitute immune cell populations for two months and
401 reconstitution was routinely assessed before any further intervention by flow cytometry.

402 *Treatment with Maraviroc*

403 Maraviroc (MedChem Express) was dissolved in 10% DMSO (Thermo Scientific,
404 20688), 40% PEG300 (Selleckchem, S6704), 5% Tween-80 (Selleckchem, S6702) and
405 45% saline and the resultant solution was sonicated. Young (3 mo) and Old (23 mo)
406 C57BL/6J HccRsd mice were assigned in three groups; young mice were i.p. daily treated
407 with vehicle and old mice were i.p. daily treated with either vehicle or 35 mg/kg
408 Maraviroc for one month.

409 **Rotarod test**

410 Motor coordination was assessed by performing the rotarod test in an accelerating rotarod
411 apparatus (Ugo Basile, Varese, Italy). Mice were trained for 1 day at a constant speed:
412 two times at 4 r.p.m. for 1 min and two times with acceleration from 4-8 r.p.m. for 1 min.
413 On the second day, the rotarod was set to progressively accelerate from 4 to 40 r.p.m for
414 5 min. Mice were tested three times. During the accelerating trials mice were video-
415 recorded and the latency to fall from the rod was measured.

416 **Forelimbs strength analysis**

417 Limb grip strength was measured as tension force using a digital force transducer (Grip
418 Strength Meter, Biobest). Ten measurements were performed for each animal, with a 10
419 second resting period between measurements and average of all measurements of every
420 mouse was compared.

421 **Metabolic cages**

422 Metabolic parameters were measured using PhenoMaster TSE-Systems (Germany). Mice
423 were singly housed and acclimatized for 1 days before data monitoring. All parameters
424 were measured continuously and simultaneously for 1 day.

425 **Tissue processing for flow cytometry**

426 Mice were euthanized with CO₂ followed by transcardiac perfusion with ice-cold PBS.
427 The indicated tissues were extracted and processed as specified:

428 **Spleen**

429 Spleen was mashed and filtered through a 70-µm cell strainer. Red blood cells were
430 removed in Erythrocyte lysis buffer (ammonium chloride 0.15 M, sodium bicarbonate
431 0.01 M, EDTA 0.1 mM) for 5 min.

432 **Blood**

433 Blood was extracted either from the facial vein or the heart in living or euthanized mice,
434 respectively. Red blood cells were removed in Erythrocyte lysis buffer for 7 min. Cells
435 were washed and stained.

436 **Peyer's Patches or lymph nodes**

437 Peyer's patches and lymph nodes were harvested from the intestine and mashed into a
438 70- μ m cell strainer. Cell suspension was centrifuged at 400 g for 5 min at 4°C. Cell pellets
439 were resuspended in 2% FBS RPMI.

440 **White adipose tissue**

441 Gonadal white adipose tissue was digested into pre-warmed 2 mg/ml BSA 2% FBS RPMI
442 supplemented with 2 mg/ml collagenase type II (Sigma, C6885) and placed under shaking
443 at 180 rpm for 40 min at 37°C. Digested tissues were vertically rested to separate fat from
444 the aqueous phases, which were obtained using a 18G syringe needle. Cell suspensions
445 were filtered through a 70- μ m cell strainer and washed with 2% FBS RPMI. Erythrocytes
446 were removed in lysis buffer for 5 min at 4°C and washed with 1 mM EDTA PBS.

447 **Liver**

448 Liver was harvested and cut into pre-warmed 25 mM Hepes 10% FBS RPMI
449 supplemented with 0.4 mg/ml collagenase type VIII (Sigma, C2139) under shaking at 180
450 rpm for 45 min at 37°C. Digested tissue was filtered through a 70- μ m cell strainer and
451 centrifuged at 350 g for 5 min at 4 °C. Red blood cells were removed in erythrocyte lysis
452 buffer for 5 min. For leucocyte enrichment, supernatants were centrifuged in a 40%/70%
453 Percoll gradient (Sigma, GE17-0891-01) at 1250 g for 30 min at RT with acceleration on
454 6 and without brake. Isolated cells were washed with PBS and resuspended in 2% FBS
455 RPMI.

456 **Bone marrow**

457 Femurs and tibias were collected. Cells from the bone marrow were obtained by
458 centrifuging the bones at 6000 g for 1 min. Red blood cells were removed in Erythrocyte
459 lysis buffer for 3 min.

460 **Flow cytometry**

461 To differentiate between live and dead cells were firstly stained with the Zombie NIR™
462 Fixable Viability Kit (BioLegend, 423106), the Zombie Yellow™ Fixable Viability Kit
463 (BioLegend, 423104) or the Ghost Dye™ Violet 540 (Tonbo Biosciences, 13-0879) for
464 20 min at 4°C. Cells were washed with FACS staining buffer (PBS supplemented with
465 2% fetal bovine serum and 1 mM EDTA) and incubated with Fc receptor blocker purified
466 rat anti-mouse anti-CD16/CD32 (BD Biosciences, 553142) for 20 min at 4°C. Cells were

467 then incubated with primary antibodies for 20 min at 4°C and were washed twice with a
468 FACS staining buffer. The following antibodies were used for surface antigen staining:

Antigen	Fluorochrome	Clone/#Catalog	Supplier	Dilution
CD8	BUV615	53-6.7	ThermoFisher	1:500
CD127 (IL-7R)	BUV737	SB/199	BD Horizon	1:200
Ly6G	BV421	1A8	Biolegend	1:400
CD186 (CXCR6)	BV421	SA051D1	Biolegend	1:100
Streptavidin	BV421	405225	Biolegend	1:500
CD38	Pacific Blue	90	Biolegend	1:500
TIM3	BV480	5D12/TIM-3	BD Biosciences	1:200
CD45.2	V500	104	Tonbo Biosciences	1:400
CD16/32	BV510	93	Biolegend	1:100
CD44	BV570	IM7	Biolegend	1:200
CD66a (CEACAM1a)	BV650	MAB-CC1	Biolegend	1:200
CD223 (LAG3)	BV650	C9B7W	Biolegend	1:100
CD62L	BV711	MEL-14	Biolegend	1:400
Ly6C	BV785	HK1.4	Biolegend	1:400
B220	FITC	RA3-6B2	Tonbo Biosciences	1:200
CD34	FITC	RAM34	BD Biosciences	1:100
CD62L	FITC	MEL-14	Tonbo Biosciences	1:400
FoxP3	FITC	Fjk-16s	Invitrogen	1:400
Ly6C	PerCP Cy5.5	HK1.4	Biolegend	1:400
CD44	PerCP Cy5.5	IM7	Tonbo Biosciences	1:200
CD45.2	PerCP Cy5.5	104	Biolegend	1:400
CD195 (CCR5)	PerCP Cy5.5	HM-CCR5	Biolegend	1:100
PD1	PerCP eFluor710	J43	Thermofisher	1:200
CD135 (FLT3)	PerCP eFluor710	A2F10	ThermoScientific	1:200
CD8	PE	53-6.7	Tonbo Biosciences	1:400
CD117 (cKit)	PE	ACK2	Tonbo Biosciences	1:200
CD184 (CXCR4)	PE	L276F12	Biolegend	1:100
CD182 (CXCR2)	PE-Dazzle 594	SA045E1	Biolegend	1:200
NKG2D	PE-Dazzle594	CX5	Biolegend	1:200
CD25	PE Cy5	PC61	Biolegend	1:400
Ly6G	PE Cy7	1A8	Biolegend	1:400
CD101	PE Cy7	Moushi101	ThermoScientific	1:200
SLAM (CD150)	PE Cy7	TC15-12F12.2	Biolegend	1:200
CD54 (ICAM-1)	PE Cy7	YN1/1.7.4	Biolegend	1:200
CX3CR1	APC	SA011F11	Biolegend	1:200
CD11b	APC	M1/70	Tonbo Biosciences	1:200
CD284 (TLR4)	APC	SA15-21	Biolegend	1:100
CD48	APC	HM48-1	Biolegend	1:200
CD11b	Red-Fluor 710	M1/70	Tonbo Biosciences	1:200
Sca-1	APC-Cy7	D7	Biolegend	1:200
CD45	APC-Cy7	30-F11	Biolegend	1:400
CD45.1	APC-Cy7	A20	Tonbo Biosciences	1:400
CD279 (PD-1)	APC-Fire750	29F.1A12	Biolegend	1:400
CD19	APC-eFluor780	eBio1D3	ThermoScientific	1:200

CD4	APC Fire810	Gk1.5	Biolegend	1:1000
B220	Biotin	RA3-6B2	Tonbo Biosciences	1:200
Ter119	Biotin	TER-119	Tonbo Biosciences	1:200
Gr-1	Biotin	RB6-8C5	Tonbo Biosciences	1:200
CD11b	Biotin	M1/70	Tonbo Biosciences	1:200
CD11c	Biotin	M418	Tonbo Biosciences	1:200
CD4	Biotin	GK1.5	Tonbo Biosciences	1:200
CD8	Biotin	53-6.7	Tonbo Biosciences	1:200
CD3	Biotin	145-2C11	Tonbo Biosciences	1:200

469 For intracellular staining, cells were fixed and permeabilized using the
470 FoxP3/Transcription Factor Staining Kit (eBioscience) for 20 min at RT in darkness.
471 Cells were then stained with the following intracellular antibodies:

Antigen	Fluorochrome	Clone/#Catalog	Supplier	Dilution
FoxP3	FITC	Fjk-16s	Invitrogen	1:150
CCL5	PE	2E9/CCL5	Biolegend	1:200
Eomes	PE-Cy7	Dan11mag	Invitrogen	1:200
Perforin	APC	S16009A	Biolegend	1:200
TOX	eFluor660	TRX10	Invitrogen	1:300
BHLHE40	Alexa Fluor 700	#NB100-1800AF700	Novus Biologicals	1:200

472 Flow cytometry experiments were performed with either a 4-laser or a 5-laser (Violet,
473 blue, yellow-green, red) Aurora flow cytometer (Cytek Biosciences). Data were analyzed
474 with the FlowJo v10.5.3 software (BD Biosciences). Gating strategies were set on the
475 basis of fluorescence minus one controls and unstained samples. All the samples in the
476 experiment excluded dead cells, clumps, and debris.

477 Analysis of mitochondrial membrane potential

478 Analysis of mitochondrial mass and mitochondrial membrane potential was performed
479 by flow cytometry in cells labelled for 30 min with 50 nM MitoTracker™ Green FM
480 (Invitrogen, M7514) and 25 nM Mitotracker™ DeepRed FM (Invitrogen, M22426) in
481 RPMI medium in a 37°C and 5% CO₂ incubator prior to extracellular staining.

482 **Dimensional reduction and clustering analysis of flow cytometry data**

483 Dimensional reduction and clustering analysis of flow cytometry data was performed
484 using OMIQ (Dotmatics). First, non-lymphocyte cells, doublets and dead cells were
485 excluded based on viability staining and FSC/SSC parameters. Then, 35,000 CD4⁺ cells
486 from each sample were subsampled for further analysis. For dimensional reduction, the
487 Uniform Manifold Approximation and Projection (UMAP) algorithm was applied with
488 the following parameters: Neighbors = 15, Minimum Distance = 0.4, Components = 2,
489 Learning Rate = 1, Epochs = 200. For unbiased clustering, the Cluster-X algorithm was

490 applied with Alpha = 0.001. The mean fluorescence intensity of each marker was
491 projected on the UMAP plots and used to infer the identity of the clusters. Similar clusters
492 were combined.

493 **Haematology**

494 The ADVIA® 2120i Hematology System (Siemens Healthineers, Erlangen, Germany)
495 was used to quantitatively measure blood variables. For ADVIA measurements, 50 µL of
496 whole blood was resuspended in 150 µL of RPMI-EDTA-K2 medium. The instrument
497 was calibrated on the day of testing as per the manufacturer's instructions.

498 **Immunohistochemistry and immunofluorescence**

499 Organs obtained from intracardiac perfused animals were fixed in 10% neutral buffered
500 formalin for 48 hr and dehydrated in 70% ethanol until processing. Dehydrated organs
501 were embedded in paraffin sections and processed with a microtome to generate x µm
502 sections. For immunostaining, the deparaffinized sections were rehydrated and boiled in
503 order to retrieve antigens (10 mM citrate buffer, 0.05% Triton X-100, pH 6). Then,
504 sections were blocked for 45 min in 10% goat serum, 5% horse serum, 0.05% TritonX-
505 100, and 2% BSA in PBS. Endogenous peroxidase and biotin were blocked with 1%
506 hydrogen peroxide-methanol for 10 min and a biotin blocking kit (Vector Laboratories),
507 respectively. Sections were incubated with a goat polyclonal anti-MPO antibody
508 (AF3667, RD Systems) and color was developed with 3,3'-diaminobenzidine (DAB,
509 Vector Laboratories). Sections were counterstained with hematoxylin and mounted in
510 DPX (Fluka). Slides were scanned with a NanoZoomer-RS scanner (Hamamatsu).
511 Briefly, for each animal, the number of MPO-positive cells was quantified in digitized
512 images in which an area covering at least one-half of a section of the whole organ was
513 previously defined. Then, the density of cells per area was estimated by using the Zen 2.3
514 software (Carl Zeiss, Inc.).

515 For immunofluorescence, after blocking, sections were instead incubated with a primary
516 mouse monoclonal anti-p16 antibody (ab54210, Abcam) followed by a Donkey anti-
517 mouse fluorophore-coupled secondary antibody (ThermoFisher).

518 **Analysis of mouse serum samples**

519 All the plasma analysis was done by Mouse Metabolism & Phenotyping core in Baylor
520 College of Medicine at Houston, Texas. Insulin, adiponectin and leptin were measured
521 by ELISA (Millipore) following manufacturer protocol.

522 **Luminex detection of proinflammatory cytokines**

523 Serum cytokines were detected with magnetic bead technology (Invitrogen, Cytokine &
524 Chemokine 26-Plex Mouse ProcartaPlex™ PanelLuminex) following manufacturer
525 instructions.

526 **RNA extraction and quantitative RT-PCR analysis**

527 *RNA extraction and reverse transcription*

528 Cultured T cells were homogenised in TRIzol® reagent (Thermo Fisher Scientific). An
529 aqueous (RNA-containing) phase was generated using 1:5 bromo-chloro-propane, mixed
530 1:2 with 70% isopropanol and centrifuged at 12,000 g to precipitate RNA. Samples were
531 treated with DNaseI (Qiagen). RNA concentration and integrity were determined by a
532 NanoDrop™ One spectrophotometer (Thermo Scientific). Total RNA with an
533 A260/A280 ratio ranging from 1.8 to 2.2 was converted to cDNA using the Maxima First
534 Strand cDNA Synthesis Kit for RT-qPCR with dsDNase (Thermo Fisher Scientific).

535 *Quantitative PCR*

536 Quantitative PCR (qPCR) primers (Invitrogen-ThermoFisher) were designed using
537 Primer-BLAST (NCBI; sequences are detailed below). A total of 10 ng of cDNA was
538 used for quantitative PCR in a total volume of 10 µl with GoTaq® qPCR Master Mix
539 (Promega) and specific primers, on a Bio-Rad CFX Opus 384 (Bio-Rad Laboratories).
540 The amplification conditions were determined by the primers to present amplification
541 efficiency close to 100% and a single peak in melt-curve analyses. Each Real-time PCR
542 reaction was performed in triplicate. Glyceraldehyde 3-phosphate dehydrogenase (*Gapdh*
543 mRNA) and β-actin (*Actb* mRNA), encoding housekeeping proteins GAPDH and β-
544 Actin, respectively, were included to monitor differences in RNA abundance. The log-
545 fold change in mRNA expression was calculated from $\Delta\Delta Ct$ values relative to control
546 samples (T cells with acute stimulation and maintained with IL-2).

Oligonucleotides for qPCR		
<i>Ccl5</i>	Thermo Fisher Scientific	F: CCTGCTGCTTGCCTACCTCTC R: ACACACTTGGCGGTTCCCTTCGA
<i>Eomes</i>	Thermo Fisher Scientific	F: GTCAACACTTGCCTCAAGC R: AAGACAGGTGGGCTCATTCT
<i>CD38</i>	Thermo Fisher Scientific	F: GGTCCAAGTGATGCTCAATGGG

		R: AGCTCCTTCGATGTCGTGCATC
<i>Pdcd1</i>	Thermo Fisher Scientific	F: CGGTTCAAGGCATGGCATTGG R: TCAGAGTGTGTCGTCTTGCTTCC
<i>Actb</i>	Thermo Fisher Scientific	F: GATGTATGAAGGCTTGGTC R: TGTGCACCTTTATTGGTCTC
<i>Gapdh</i>	Thermo Fisher Scientific	F: CATCACTGCCACCCAGAAGACTG R: ATGCCAGTGAGCTTCCCAGTCAG

547 **Statistical analysis**

548 Statistical analysis was performed with GraphPad Prism (version 9). Data are expressed
549 as mean \pm s.e.m. (standard error of the mean). Outliers were excluded by the ROUT
550 method (5%). Comparisons for two groups were calculated using unpaired two-tailed
551 Student's *t*-tests (for two groups meeting the normal distribution criteria) or Mann-
552 Whitney U test (for two groups without normal distribution) according to the Shapiro-
553 Wilk normality test. Comparisons for more than three groups were calculated using One-
554 Way ANOVA (for three or more groups meeting the normal distribution criteria) or
555 Kruskal-Wallis test (for three or more groups without normal distribution) according to
556 the Shapiro-Wilk normality test.

557 Unless otherwise specified, *n* represents the number of individual biological replicates
558 and is represented in graphs as one dot per sample. Flow cytometry plots are
559 representative of at least three replicates. No statistical method was used to predetermine
560 sample size, but a minimum of three samples were used per experimental group and
561 condition.

562 References

- 563 1 Van Avondt, K. *et al.* Neutrophils in aging and aging-related pathologies. *Immunol Rev* **314**,
564 357-375 (2023). <https://doi.org/10.1111/imr.13153>
- 565 2 Fest, J. *et al.* The neutrophil-to-lymphocyte ratio is associated with mortality in the general
566 population: The Rotterdam Study. *Eur J Epidemiol* **34**, 463-470 (2019).
<https://doi.org/10.1007/s10654-018-0472-y>
- 568 3 Li, J. *et al.* Neutrophil-to-Lymphocyte Ratio Positively Correlates to Age in Healthy
569 Population. *J Clin Lab Anal* **29**, 437-443 (2015). <https://doi.org/10.1002/jcla.21791>
- 570 4 Pellegrino, R. *et al.* Neutrophil, lymphocyte count, and neutrophil to lymphocyte ratio
571 predict multimorbidity and mortality-results from the Baltimore Longitudinal Study on
572 Aging follow-up study. *Geroscience* (2024). <https://doi.org/10.1007/s11357-023-01034-7>
- 573 5 Song, M., Graubard, B. I., Rabkin, C. S. & Engels, E. A. Neutrophil-to-lymphocyte ratio and
574 mortality in the United States general population. *Sci Rep* **11**, 464 (2021).
<https://doi.org/10.1038/s41598-020-79431-7>
- 576 6 Desdín-Micó, G. *et al.* T cells with dysfunctional mitochondria induce multimorbidity and
577 premature senescence. *Science* **368**, 1371-1376 (2020).
<https://doi.org/10.1126/science.aax0860>
- 579 7 Furman, D. *et al.* Chronic inflammation in the etiology of disease across the life span. *Nat
580 Med* **25**, 1822-1832 (2019). <https://doi.org/10.1038/s41591-019-0675-0>
- 581 8 Sayed, N. *et al.* An inflammatory aging clock (iAge) based on deep learning tracks
582 multimorbidity, immunosenescence, frailty and cardiovascular aging. *Nat Aging* **1**, 598-615
583 (2021). <https://doi.org/10.1038/s43587-021-00082-y>
- 584 9 Soehnlein, O., Steffens, S., Hidalgo, A. & Weber, C. Neutrophils as protagonists and targets
585 in chronic inflammation. *Nat Rev Immunol* **17**, 248-261 (2017).
<https://doi.org/10.1038/nri.2017.10>
- 587 10 Barkaway, A. *et al.* Age-related changes in the local milieu of inflamed tissues cause
588 aberrant neutrophil trafficking and subsequent remote organ damage. *Immunity* **54**, 1494-
589 1510.e1497 (2021). <https://doi.org/10.1016/j.immuni.2021.04.025>
- 590 11 Lagnado, A. *et al.* Neutrophils induce paracrine telomere dysfunction and senescence in
591 ROS-dependent manner. *Embo J* **40**, e106048 (2021).
<https://doi.org/10.15252/embj.2020106048>
- 593 12 Ho, Y. H. *et al.* Remodeling of Bone Marrow Hematopoietic Stem Cell Niches Promotes
594 Myeloid Cell Expansion during Premature or Physiological Aging. *Cell Stem Cell* **25**, 407-
595 418.e406 (2019). <https://doi.org/10.1016/j.stem.2019.06.007>
- 596 13 Collins, N. *et al.* The Bone Marrow Protects and Optimizes Immunological Memory during
597 Dietary Restriction. *Cell* **178**, 1088-1101.e1015 (2019).
<https://doi.org/10.1016/j.cell.2019.07.049>
- 599 14 Poller, W. C. *et al.* Brain motor and fear circuits regulate leukocytes during acute stress.
600 *Nature* **607**, 578-584 (2022). <https://doi.org/10.1038/s41586-022-04890-z>
- 601 15 Shi, K. *et al.* Bone marrow hematopoiesis drives multiple sclerosis progression. *Cell* **185**,
602 2234-2247.e2217 (2022). <https://doi.org/10.1016/j.cell.2022.05.020>
- 603 16 Wang, L. *et al.* Fasting-activated ventrolateral medulla neurons regulate T cell homing and
604 suppress autoimmune disease in mice. *Nat Neurosci* (2024). <https://doi.org/10.1038/s41593-023-01543-w>
- 606 17 Casanova-Acebes, M. *et al.* Rhythmic modulation of the hematopoietic niche through
607 neutrophil clearance. *Cell* **153**, 1025-1035 (2013). <https://doi.org/10.1016/j.cell.2013.04.040>
- 608 18 Zhang, D. *et al.* Neutrophil ageing is regulated by the microbiome. *Nature* **525**, 528-532
609 (2015). <https://doi.org/10.1038/nature15367>
- 610 19 Mombaerts, P. *et al.* RAG-1-deficient mice have no mature B and T lymphocytes. *Cell* **68**,
611 869-877 (1992). [https://doi.org/10.1016/0092-8674\(92\)90030-g](https://doi.org/10.1016/0092-8674(92)90030-g)
- 612 20 Elyahu, Y. *et al.* Aging promotes reorganization of the CD4 T cell landscape toward extreme
613 regulatory and effector phenotypes. *Sci Adv* **5**, eaaw8330 (2019).
<https://doi.org/10.1126/sciadv.aaw8330>

615 21 Mogilenko, D. A. *et al.* Comprehensive Profiling of an Aging Immune System Reveals
616 Clonal GZMK(+) CD8(+) T Cells as Conserved Hallmark of Inflammaging. *Immunity* **54**,
617 99-115.e112 (2021). <https://doi.org/10.1016/j.immuni.2020.11.005>

618 22 Mittelbrunn, M. & Kroemer, G. Hallmarks of T cell aging. *Nat Immunol* **22**, 687-698 (2021).
619 <https://doi.org/10.1038/s41590-021-00927-z>

620 23 Vardhana, S. A. *et al.* Impaired mitochondrial oxidative phosphorylation limits the self-
621 renewal of T cells exposed to persistent antigen. *Nat Immunol* **21**, 1022-1033 (2020).
622 <https://doi.org/10.1038/s41590-020-0725-2>

623 24 Baixaulli, F. *et al.* Mitochondrial Respiration Controls Lysosomal Function during
624 Inflammatory T Cell Responses. *Cell Metab* **22**, 485-498 (2015).
625 <https://doi.org/10.1016/j.cmet.2015.07.020>

626 25 Barnden, M. J., Allison, J., Heath, W. R. & Carbone, F. R. Defective TCR expression in
627 transgenic mice constructed using cDNA-based alpha- and beta-chain genes under the
628 control of heterologous regulatory elements. *Immunol Cell Biol* **76**, 34-40 (1998).
629 <https://doi.org/10.1046/j.1440-1711.1998.00709.x>

630 26 Kantor, R., Bakhashvili, M. & Achiron, A. A mutated CCR5 gene may have favorable
631 prognostic implications in MS. *Neurology* **61**, 238-240 (2003).
632 <https://doi.org/10.1212/01.wnl.0000069921.20347.9e>

633 27 Lieberman-Blum, S. S., Fung, H. B. & Bandres, J. C. Maraviroc: a CCR5-receptor
634 antagonist for the treatment of HIV-1 infection. *Clin Ther* **30**, 1228-1250 (2008).
635 [https://doi.org/10.1016/s0149-2918\(08\)80048-3](https://doi.org/10.1016/s0149-2918(08)80048-3)

636 28 Hashimoto, K. *et al.* Single-cell transcriptomics reveals expansion of cytotoxic CD4 T cells
637 in supercentenarians. *Proc Natl Acad Sci U S A* **116**, 24242-24251 (2019).
638 <https://doi.org/10.1073/pnas.1907883116>

639 29 Takeuchi, A. & Saito, T. CD4 CTL, a Cytotoxic Subset of CD4(+) T Cells, Their
640 Differentiation and Function. *Front Immunol* **8**, 194 (2017).
641 <https://doi.org/10.3389/fimmu.2017.00194>

642 30 Hasegawa, T. *et al.* Cytotoxic CD4(+) T cells eliminate senescent cells by targeting
643 cytomegalovirus antigen. *Cell* **186**, 1417-1431.e1420 (2023).
644 <https://doi.org/10.1016/j.cell.2023.02.033>

645 31 Oh, D. Y. & Fong, L. Cytotoxic CD4(+) T cells in cancer: Expanding the immune effector
646 toolbox. *Immunity* **54**, 2701-2711 (2021). <https://doi.org/10.1016/j.immuni.2021.11.015>

647 32 Maryanovich, M. *et al.* Adrenergic nerve degeneration in bone marrow drives aging of the
648 hematopoietic stem cell niche. *Nat Med* **24**, 782-791 (2018). <https://doi.org/10.1038/s41591-018-0030-x>

649 33 Mitchell, C. A. *et al.* Stromal niche inflammation mediated by IL-1 signalling is a targetable
650 driver of haematopoietic ageing. *Nat Cell Biol* **25**, 30-41 (2023).
651 <https://doi.org/10.1038/s41556-022-01053-0>

652 34 Young, K. *et al.* Decline in IGF1 in the bone marrow microenvironment initiates
653 hematopoietic stem cell aging. *Cell Stem Cell* **28**, 1473-1482.e1477 (2021).
654 <https://doi.org/10.1016/j.stem.2021.03.017>

655 35 Kusumbe, A. P. *et al.* Age-dependent modulation of vascular niches for haematopoietic stem
656 cells. *Nature* **532**, 380-384 (2016). <https://doi.org/10.1038/nature17638>

657 36 Ambrosi, T. H. *et al.* Adipocyte Accumulation in the Bone Marrow during Obesity and
658 Aging Impairs Stem Cell-Based Hematopoietic and Bone Regeneration. *Cell Stem Cell* **20**,
659 771-784.e776 (2017). <https://doi.org/10.1016/j.stem.2017.02.009>

660 37 Adrover, J. M. *et al.* A Neutrophil Timer Coordinates Immune Defense and Vascular
661 Protection. *Immunity* **51**, 966-967 (2019). <https://doi.org/10.1016/j.immuni.2019.11.001>

662 38 Chen, J. *et al.* CREB1-driven CXCR4(hi) neutrophils promote skin inflammation in mouse
663 models and human patients. *Nat Commun* **14**, 5894 (2023). <https://doi.org/10.1038/s41467-023-41484-3>

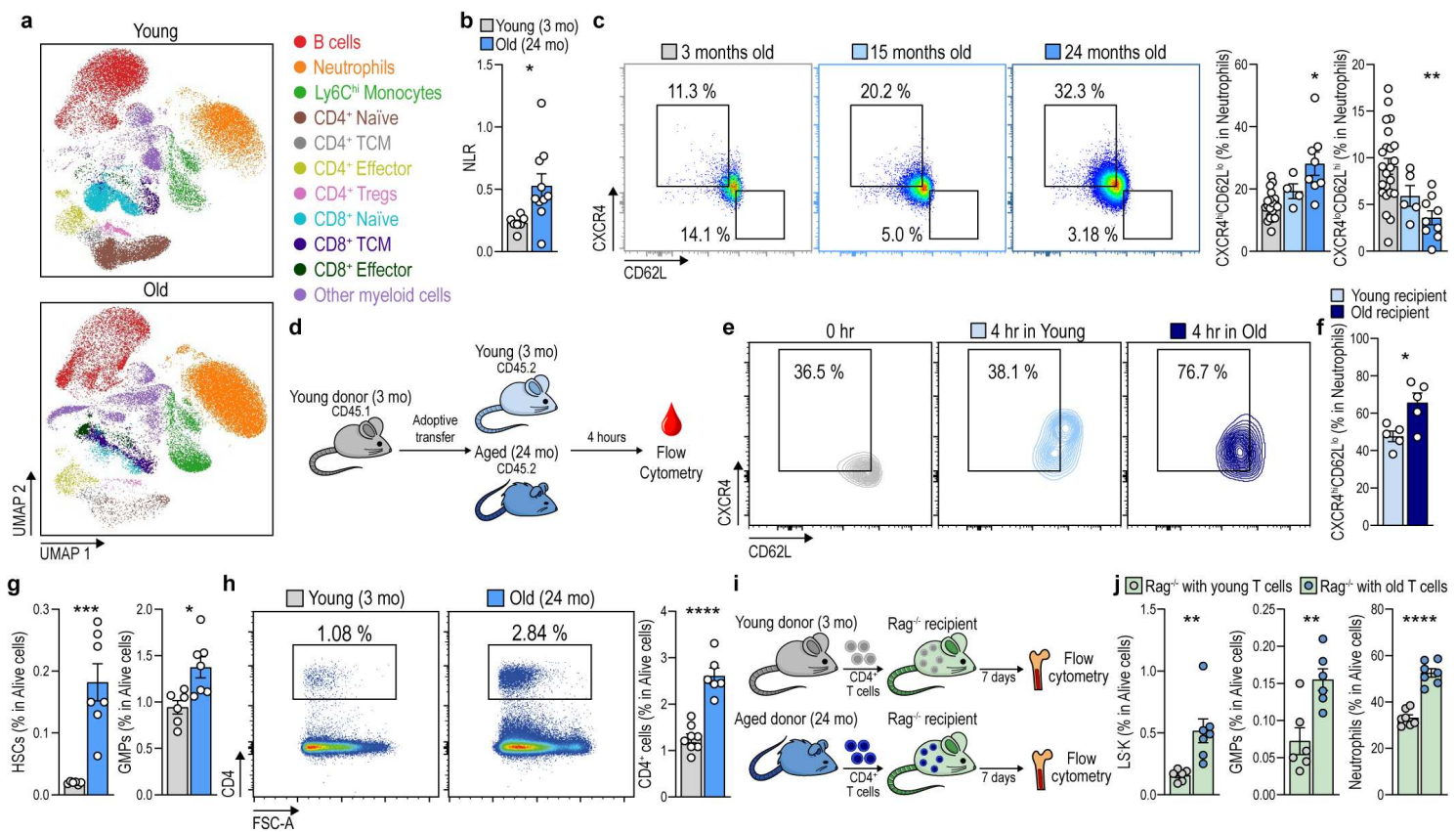
664 39 Joy, M. T. *et al.* CCR5 Is a Therapeutic Target for Recovery after Stroke and Traumatic
665 Brain Injury. *Cell* **176**, 1143-1157.e1113 (2019). <https://doi.org/10.1016/j.cell.2019.01.044>

668 40 Gullotta, G. S. *et al.* Age-induced alterations of granulopoiesis generate atypical neutrophils
669 that aggravate stroke pathology. *Nat Immunol* **24**, 925-940 (2023).
670 <https://doi.org/10.1038/s41590-023-01505-1>

671 41 Larsson, N. G. *et al.* Mitochondrial transcription factor A is necessary for mtDNA
672 maintenance and embryogenesis in mice. *Nat Genet* **18**, 231-236 (1998).
673 <https://doi.org/10.1038/ng0398-231>

674 **Figures**

675 **Figure 1**

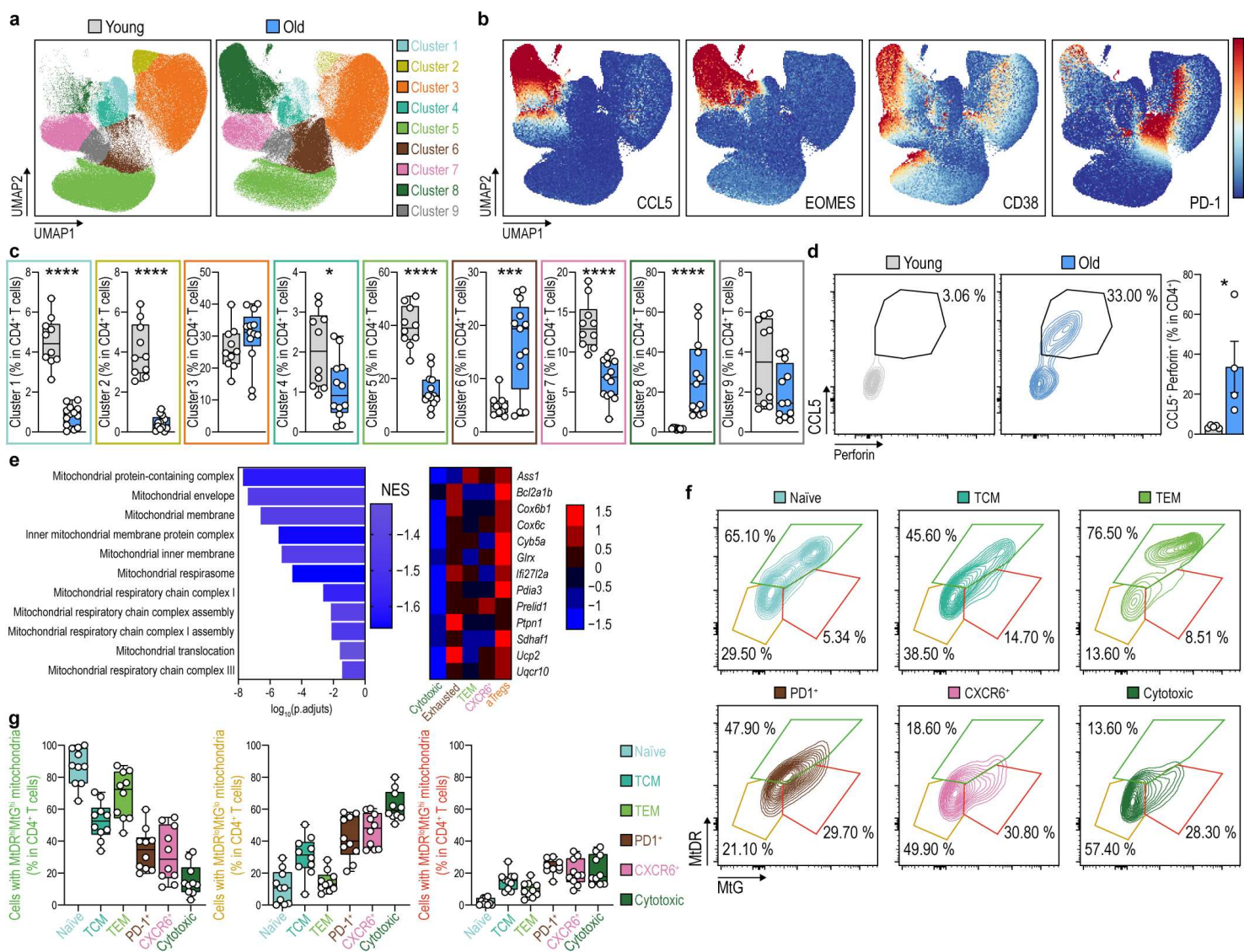


676 **Figure 1 | Accumulation of CD4⁺ T cells in the bone marrow leads to enhanced**
677 **granulopoiesis and increased levels of pro-inflammatory neutrophils in aged mice.**

678 **a**, UMAP with Cluster-X overlay showing the distribution of the clusters of immune cells
679 identified by multiparametric spectral flow cytometry in the circulation of young (3
680 months old, mo) and old (24 mo) mice. **b**, Quantification of the NLR in the circulation of
681 young (3 mo) and old (24 mo) mice (n = 7-10 mice per group). **c**, Representative dot
682 plots and quantification of CXCR4^{hi} CD62L^{lo} and CXCR4^{lo} CD62L^{hi} neutrophils in the
683 circulation of young (3 mo) middle-aged (15 mo) and old (24 mo) mice (n = 4-23 mice
684 per group). **d**, Schematic diagram depicting the adoptive transfer of blood from 3 mo
685 CD45.1⁺ mice into either young (3 mo) or old (24 mo) CD45.2⁺ recipients. **e,f**, Contour
686 plot (e) and quantification (f) showing CD45.1⁺ CXCR4^{hi} CD62L^{lo} transferred
687 neutrophils before (0 hr) and after (4 hr) the adoptive transfer into either young (3 mo) or
688 old (24 mo) mice (n = 5 mice per group). **g**, Percentage of HSCs, and GMPs in the BM
689 from young (3 mo) and old (24 mo) mice assessed by flow cytometry (n = 6-8 mice per
690 group). **h**, Representative flow cytometry plots and quantification of the percentage of
691 CD4⁺ cells in the BM of young (3 mo) and old (24 mo) mice. **i**, Schematic diagram

692 depicting the adoptive transfer of CD4⁺ cells isolated from young (3 mo) or old (24 mo)
693 into young *Rag1*^{-/-} recipients. **j**, Quantification of the percentage of LS⁻K, GMPs and
694 neutrophils in the BM of recipient animals 7 days after the adoptive transfer (n = 6-7 mice
695 per group).

696 **Figure 2**

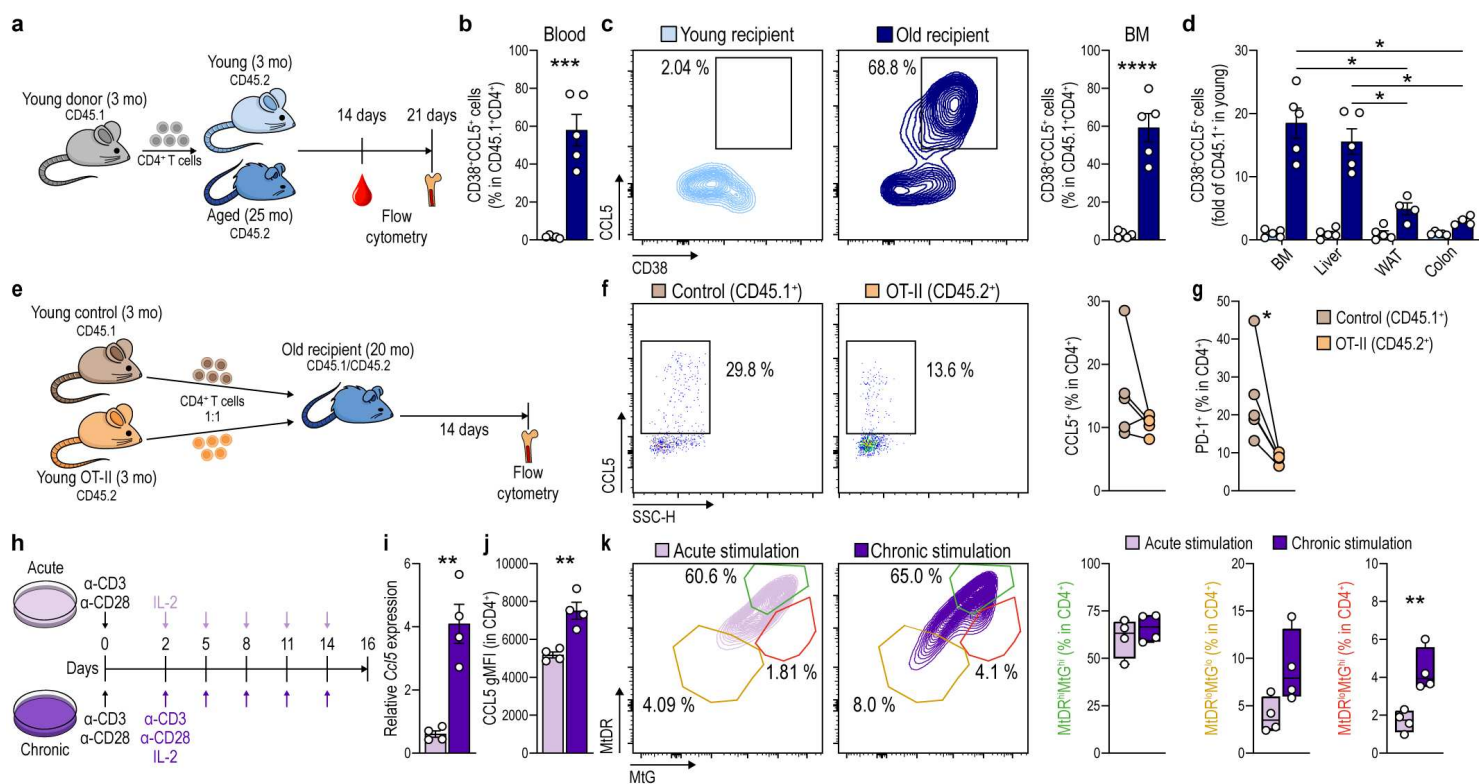


697 **Figure 2 | CD4⁺ T cells accumulating in the aged bone marrow exhibit a cytotoxic profile and harbour dysfunctional mitochondria.**

699 **a**, UMAP with Cluster-X overlay showing the distribution of the nine clusters of CD4⁺ T cells identified by multiparametric spectral flow cytometry in the BM from young (3 months old, mo) and old (24 mo) mice. **b**, UMAP representation of the expression levels of representative markers used to identify the CD4⁺ CTLs. **c**, Boxplots comparing the percentage of cells in each T cell subset in young (3 mo) and old (20 mo) mice (n = 10-13 mice per group). **d**, Representative flow cytometry plots and quantification of the percentage of CCL5⁺ Perforin⁺ CD4⁺ cells in the BM of young (3 mo) and old (24 mo) mice (n = 4-5 mice per group). **e**, GSEA analysis of differentially expressed pathways related to mitochondrial function in CD4⁺ CTLs compared with the other differentiated CD4⁺ cells (left) and heat map showing the expression of differentially expressed genes

709 between the different clusters (right). **f**, Representative contour plots showing MtDR and
710 MtG in the clusters identified by extracellular staining in BM CD4⁺ cells from old (24
711 mo) mice (n = 10 mice per group). **g**, Quantification of the percentage of BM T cells
712 exhibiting healthy (MtDR^{hi}MtG^{lo}, left), depolarized (MtDR^{lo}MtG^{lo}, middle) or
713 (MtDR^{lo}MtG^{hi}, right) mitochondria in the different clusters.

714 **Figure 3**

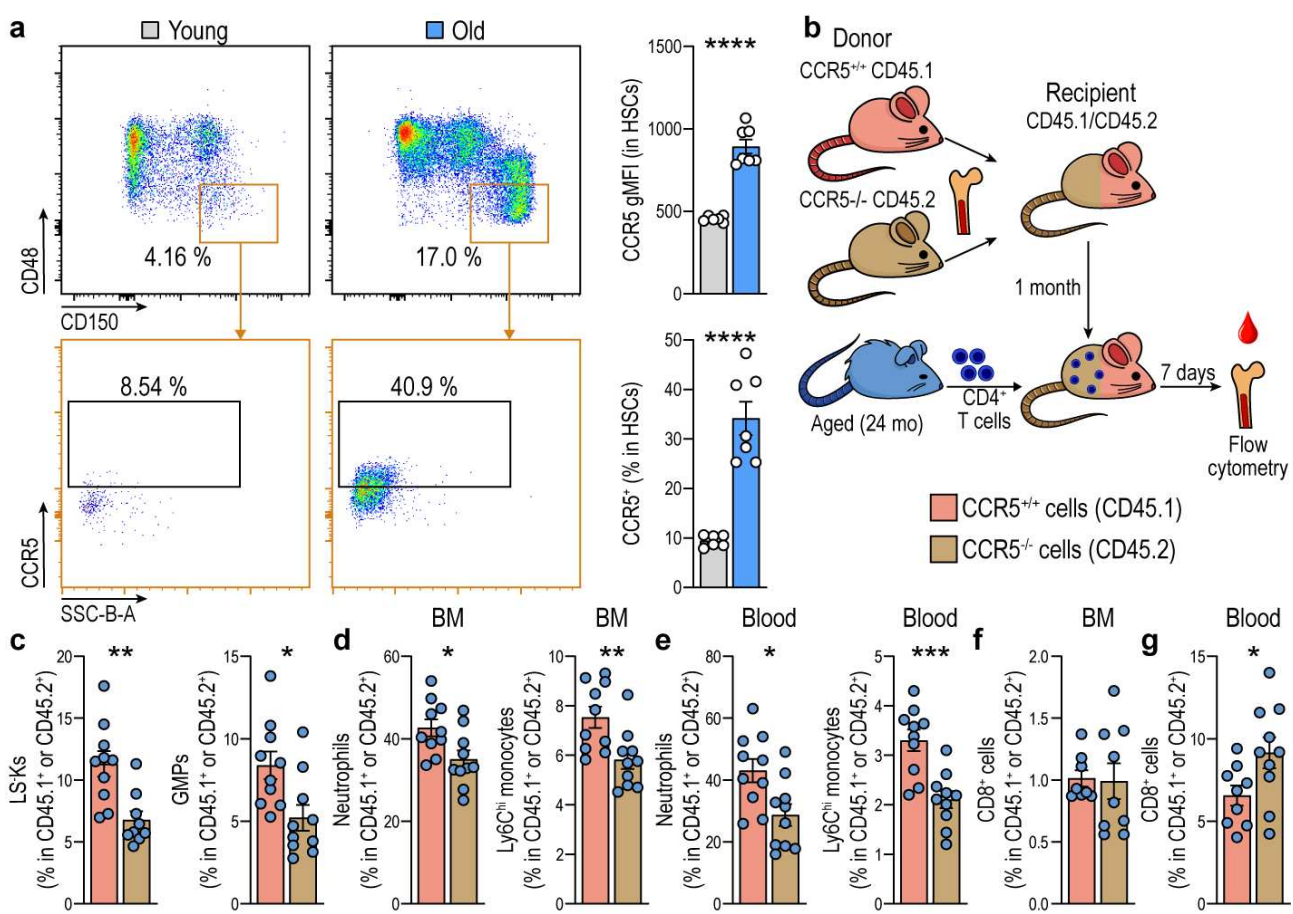


715 **Figure 3 | Prolonged TCR engagement in an aged environment induces mitochondrial dysfunction and CD4⁺ CTL differentiation.**

717 **a**, Schematic diagram depicting the adoptive transfer of CD45.1⁺ T cells isolated from 3
718 months old (mo) mice into either young (3 mo) or old (24 mo) CD45.2⁺ recipients. **b**,
719 Percentage of blood CD4⁺CD38⁺CCL5⁺ T cells in young or old recipients 21 days after
720 the adoptive transfer of CD4⁺ T cells (n = 5 mice per group). **c**, Representative contour
721 plots and quantification of the percentage of BM CD4⁺CD38⁺CCL5⁺ T cells in young or
722 old recipients 21 days after the adoptive transfer of CD4⁺ T cells (n = 5 mice per group).
723 **d**, Fold increase of CD4⁺CD38⁺CCL5⁺ T cells in the indicated organs from young and
724 old recipients (n = 5 mice per group). **e**, Schematic diagram depicting the mixed adoptive
725 transfer of CD45.1⁺ control and CD45.2⁺ OT-II derived cells into old (20 mo) recipients.
726 **f**, Representative dot plots and quantification of the percentage of BM CCL5⁺ CD4⁺ cells
727 in either CD45.1⁺ control or CD45.2⁺ OT-II 14 days after the adoptive transfer (n = 5
728 mice per group). **g**, Percentage of CD4⁺ PD-1⁺ cells in CD45.1⁺ control or CD45.2⁺ OT-
729 II transferred cells (n = 5 mice per group). **h**, Schematic diagram depicting the protocol
730 followed to acutely and chronically stimulate isolated CD4⁺ T cells in culture by exposure
731 to anti-CD3/anti-CD28 and IL-2. **i,j**, Levels of *Ccl5* mRNA (**i**) and CCL5 protein (**j**) in
732 acutely and chronically stimulated T cells determined by RT-qPCR analysis and flow

733 cytometry, respectively (n = 4). **k**, Representative contour plots showing MtDR and MtG
734 and quantification of the percentage of CD4⁺ cells exhibiting healthy (MtDR^{hi}MtG^{lo}) or
735 depolarized (MtDR^{lo}MtG^{lo} or MtDR^{lo}MtG^{hi}) mitochondria in acutely stimulated versus
736 chronically stimulated conditions (n = 4).

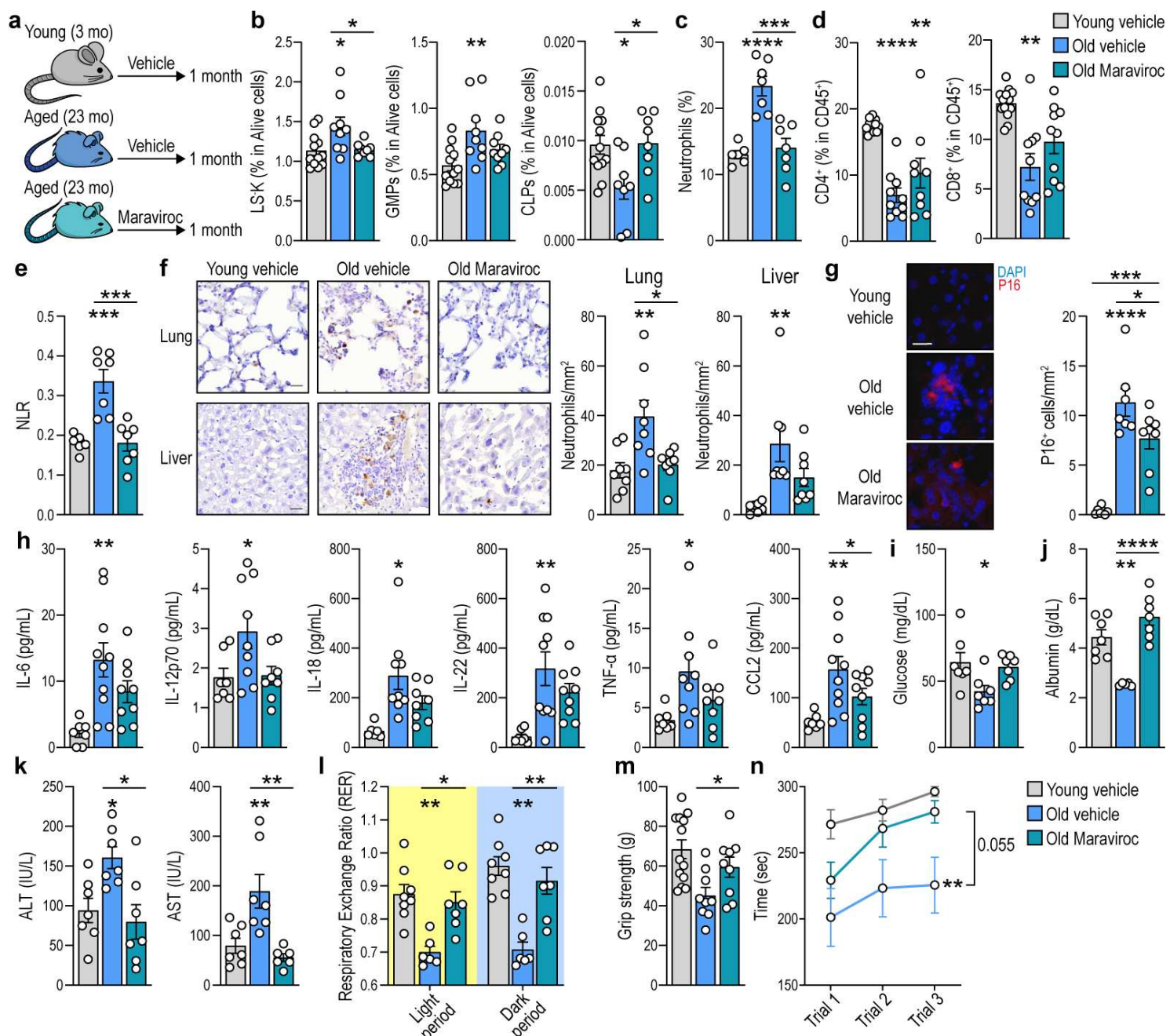
737 **Figure 4**



738 **Figure 4 | T cells from aged mice induce granulopoiesis via CCL5/CCR5.**

739 **a**, Representative dot plots showing the identification of CCR5⁺ HSCs and quantification
740 of the levels of CCR5 and the percentage of CCR5⁺ HSCs in the BM of young (3 months
741 old, mo) and old (24 mo) mice (n = 5-7 per group). **b**, Schematic diagram depicting the
742 strategy followed to generate mixed BM chimeric mice. CCR5^{+/+} (CD45.1⁺) and CCR5-
743 ^{-/-} (CD45.2⁺) derived BM cells were mixed 1:1 and i.v. injected into lethally irradiated
744 young (5-6 mo) CD45.1.2⁺ recipients. One month after transplantation, CD4⁺ CD45.2⁺
745 isolated from old (24 mo) mice were adoptively transferred into the mixed chimeric
746 recipients. **c,d**, Quantification of the percentage of LS-K and GMPs (**c**), neutrophils and
747 Ly6C^{hi} monocytes (**d**) in CCR5^{+/+} CD45.1⁺ or CCR5^{-/-} CD45.2⁺ cells into the BM of
748 mixed chimeric recipients (n = 10 mice per group). **e**, Quantification of the percentage of
749 circulating neutrophils and Ly6C^{hi} monocytes in mixed chimeric recipients (n = 10 mice
750 per group). **f,g** Percentage of CD8⁺ cells in the BM (**f**) and the blood (**g**) of mixed chimeric
751 recipients (n = 10 mice per group).

752 **Figure 5**



753 **Figure 5 | Pharmacological inhibition of CCR5 restores granulopoiesis and improves health status in aged mice.**

754 **a**, Schematic diagram detailing the treatment with Maraviroc. Old mice were either daily
755 treated with vehicle or Maraviroc for one month. Young mice were treated in parallel. **b**, Percentage of GMPs, LS-K and CLPs in the BM of the three experimental groups (n = 9-12 mice per group). **c**, Percentage of blood neutrophils in the experimental groups measured by blood haematology (n = 6-7 mice per group). **d**, Percentage CD4⁺ and CD8⁺ cells in CD45⁺ cells measured by flow cytometry in blood samples from the experimental groups (n = 9-12 mice per group). **e**, NLR in blood from the experimental groups (n = 6-7 mice per group). **f**, Immunohistochemical images of lung and liver tissue sections from young, old vehicle, and old Maraviroc mice. **g**, Immunofluorescence images of lung and liver tissue sections showing P16⁺ (red) and DAPI (blue) staining. **h**, Bar charts showing cytokine levels (IL-6, IL-12p70, IL-18, IL-22, TNF- α , CCL2) in the blood of young and aged mice treated with vehicle or Maraviroc. **i**, Bar charts showing glucose and albumin levels in the blood of young and aged mice treated with vehicle or Maraviroc. **j**, Bar charts showing ALT and AST levels in the blood of young and aged mice treated with vehicle or Maraviroc. **k**, Bar charts showing the Respiratory Exchange Ratio (RER) during Light and Dark periods for young and aged mice treated with vehicle or Maraviroc. **l**, Bar chart showing grip strength in young and aged mice treated with vehicle or Maraviroc. **m**, Line graph showing the time taken for grip strength in young and aged mice treated with vehicle or Maraviroc.

762 7 mice per group). **f**, MPO immunohistochemistry and quantification of MPO⁺ cells per
763 mm² in liver and lung sections from all experimental groups (n = 8 mice per group). **g**,
764 Immunofluorescence staining for p16 and quantification of p16⁺ cells in liver sections
765 from the experimental groups (n = 8 mice per group). Scale bar, 20 μ m. **h**, Serum levels
766 of the indicated cytokines and chemokines detected by multiplex in the three experimental
767 groups (n = 7 to 9 mice per group). **i**, Serum glucose levels in non-fasted mice from the
768 experimental groups (n = 7 mice per group). **j**, Serum albumin levels in non-fasted mice
769 from the experimental groups (n = 7 mice per group). **k**, Serum ALT and AST levels in
770 non-fasted mice from the experimental groups (n = 7 mice per group). **l**, Respiratory
771 exchange ratio (VCO₂/VO₂) assessed in metabolic cages during the light and dark phases
772 among the specified experimental groups (n = 6-8 mice per group). **m**, Quantification of
773 forelimbs strength in the three experimental groups (n = 9-13 mice per group). **n**,
774 Quantification of the latency to fall in the rotarod test in the three experimental groups (n
775 = 6-10 mice per group).

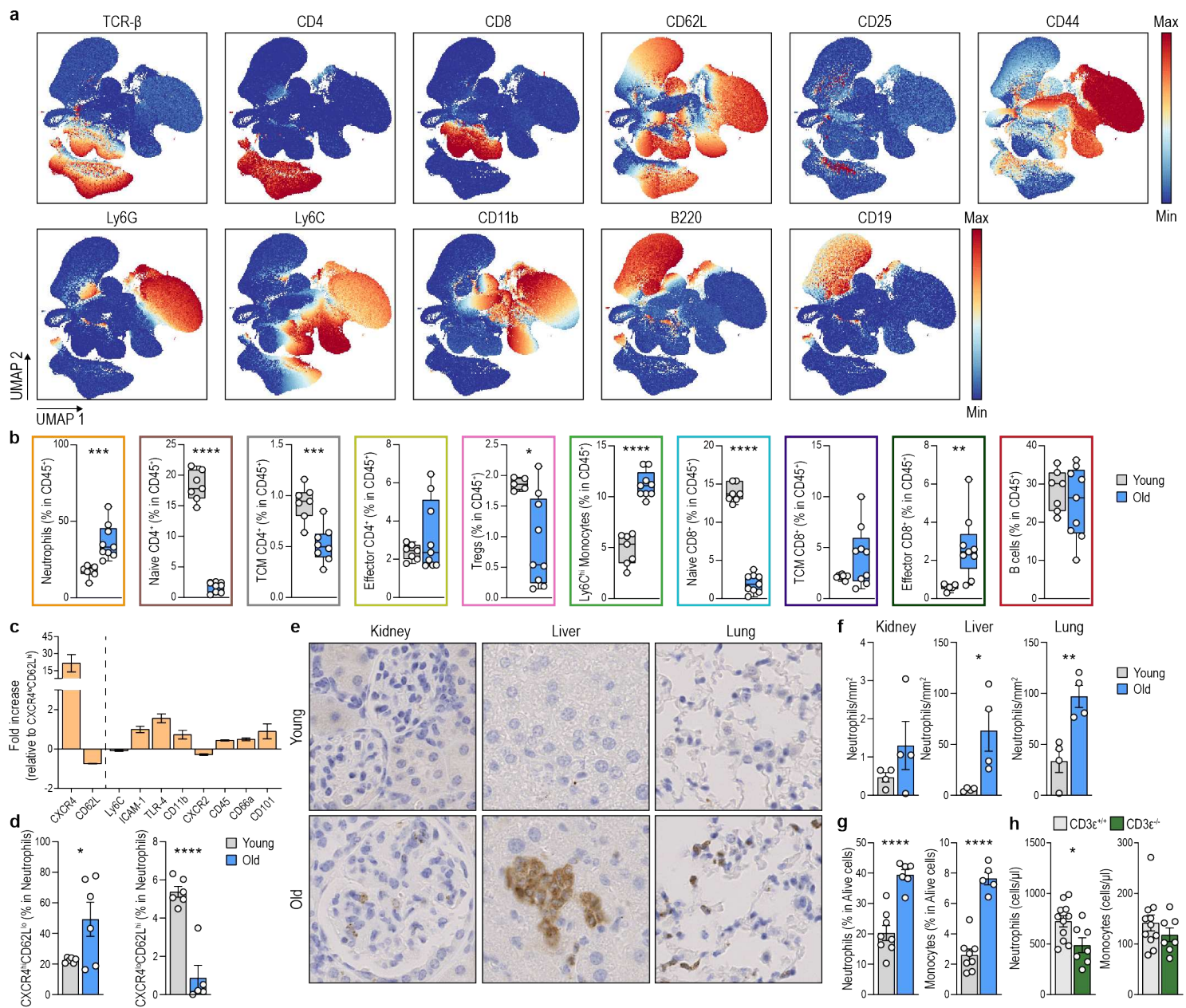
776 **Legends to supplementary material**

777 **Extended Data Table 1. Statistic comparison of Extended Data Figure 6b,d**

778 **Extended Data Table 2. Statistic comparison of Figure 2g**

779

780 **Extended Data Figure 1**

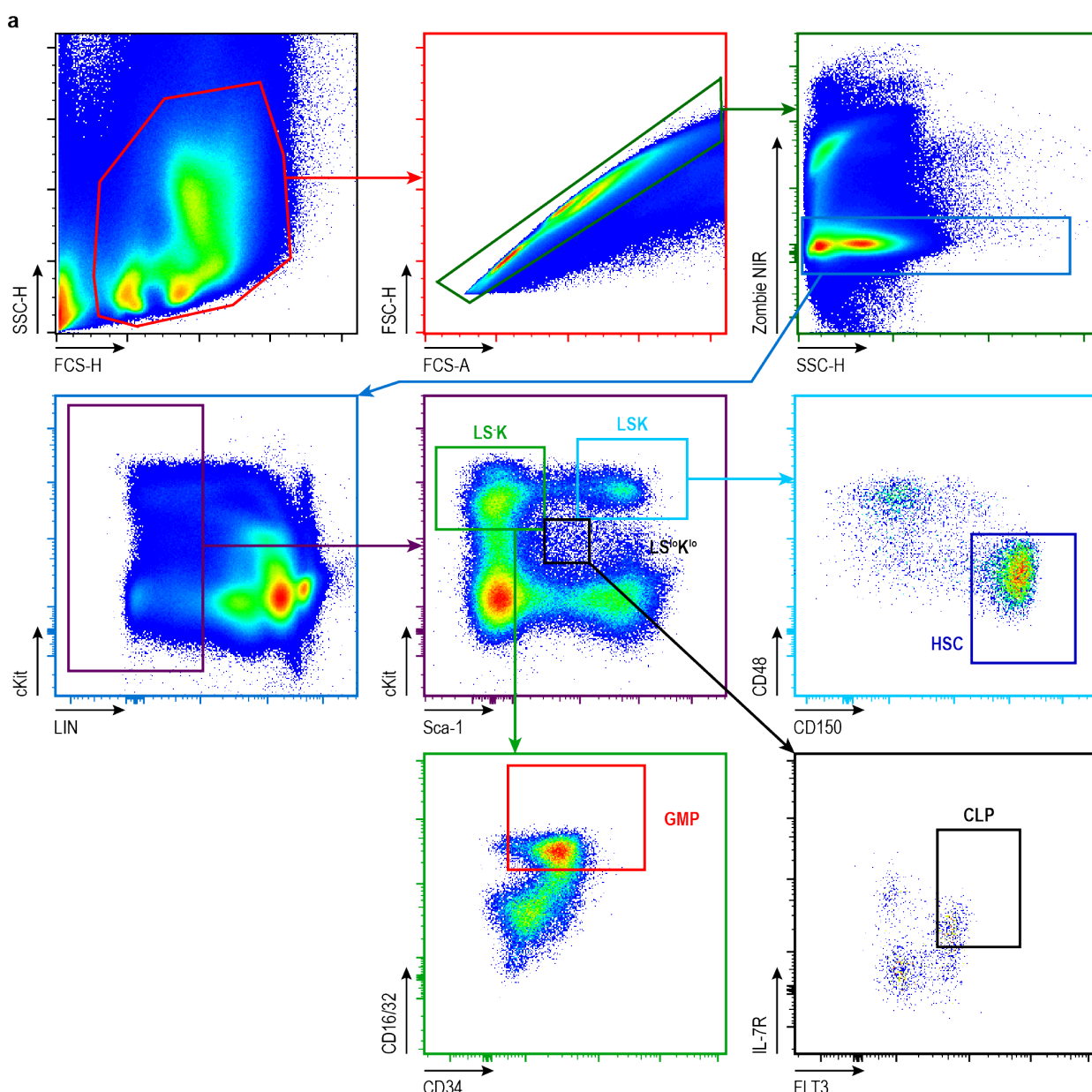


781 **Extended Data Figure 1 | Enhanced granulopoiesis and accumulation of**
 782 ***CXCR4*^{hi}*CD62L*^{lo} neutrophils in tissues from aged mice**

783 **a**, UMAP representation of the expression levels of markers used to identify the different
 784 populations of blood cells shown in Fig. 1a and Extended Fig. 7c. **b**, Boxplots comparing
 785 the percentage of the different clusters in blood from young (3 mo) and old (24 mo) mice

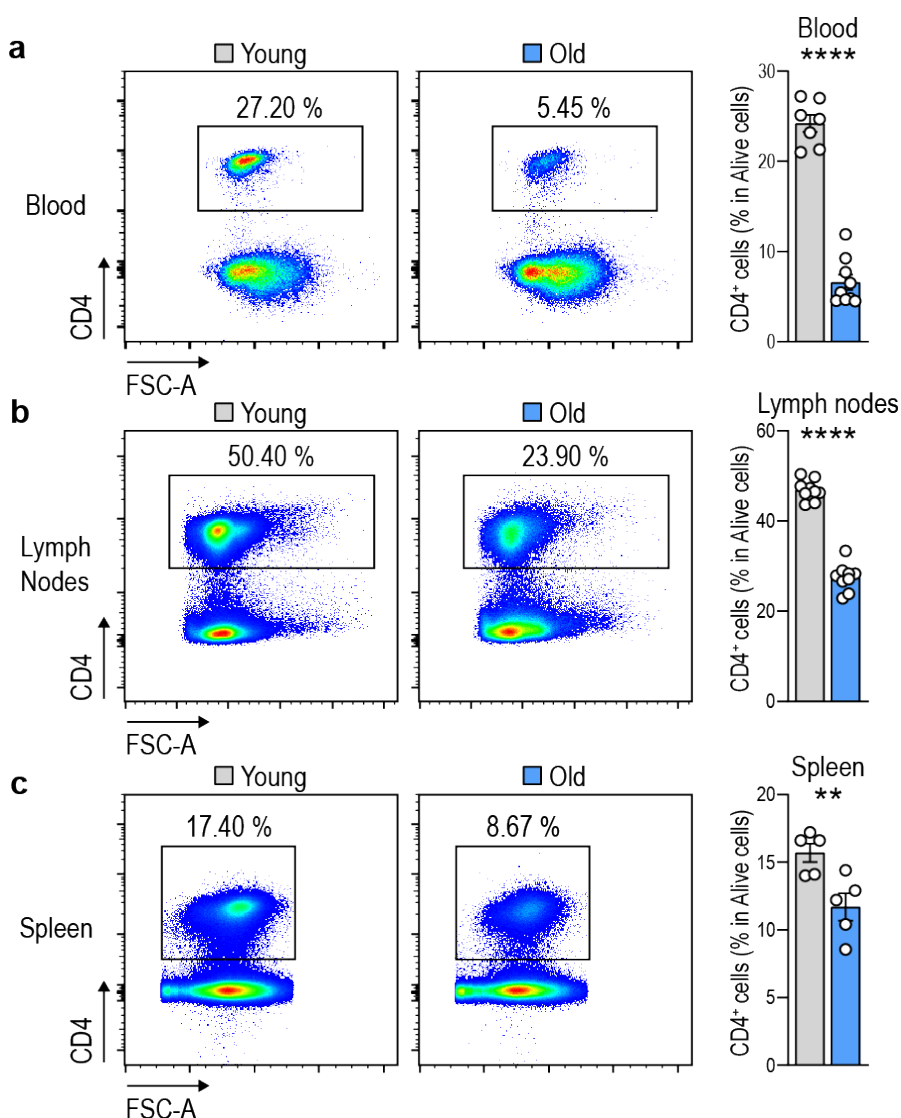
786 (n = 6-9 mice per group). **c**, Relative CXCR4^{lo} CD62L^{hi} to CXCR4^{hi} CD62L^{lo} expression
787 of different surface markers showing an upregulation of pro-inflammatory markers in
788 CXCR4^{hi} CD62L^{lo} neutrophils (n = 6-16 mice per group). **d**, Quantification of the
789 percentage of CXCR4^{hi} CD62L^{lo} and CXCR4^{lo} CD62L^{hi} neutrophils in spleen from
790 young (3 months old, mo) and old (24 mo) mice (n = 6 mice per group). **e,f**,
791 Representative immunohistochemistry images (**e**) and quantification (**f**) of
792 myeloperoxidase-positive neutrophils in kidney, liver, and lung sections from young (3
793 mo) and old (24 mo) mice (n = 4 mice per group). **g**, Percentage of neutrophils and Ly6C^{hi}
794 monocytes in the BM from young (3 mo) and old (24 mo) mice assessed by flow
795 cytometry (n = 6-8 mice per group). **h**, Percentage of neutrophils and Ly6C^{hi} monocytes
796 in blood from old (17 mo) T cell deficient *Cd3e*^{-/-} and control mice (n = 7-11 mice per
797 group).

798 **Extended Data Figure 2**



801 **a**, Gating strategy followed to identify LS⁻K (Lineage⁻Sca⁻cKit⁺) cells, GMPs (LS⁻K; CD16/32⁺CD34⁺), LSK (Lineage⁻Sca⁺cKit⁺) cells, HSCs (LSK; CD48⁺CD150⁻), LS^{lo}K^{lo} (Lineage⁻Sca^{lo}cKit^{lo}) cells and CLPs (LS^{lo}K^{lo}; IL-7R⁺FLT3⁺).

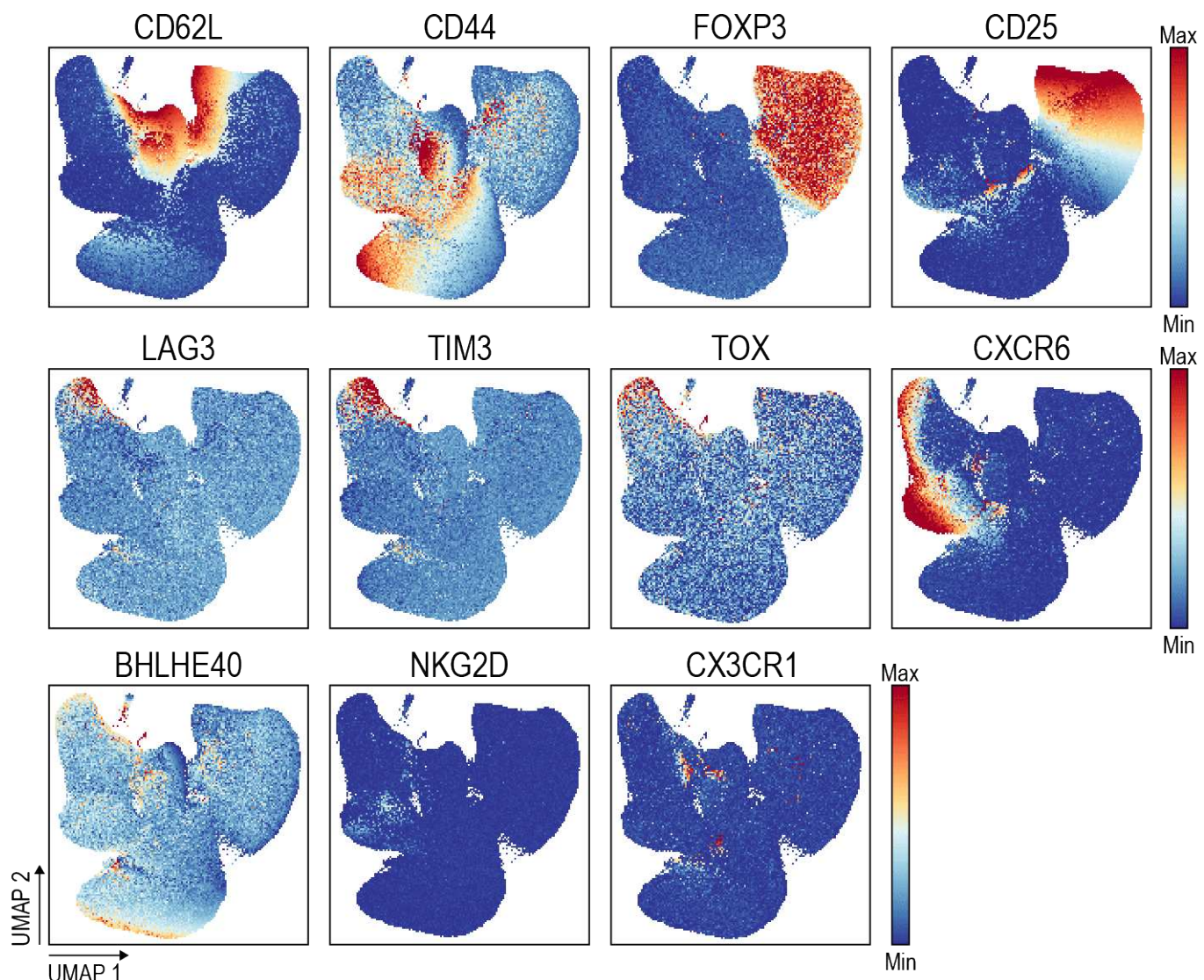
804 **Extended Data Figure 3**



805 **Extended Data Figure 3 | Decreased percentage of CD4⁺ T cells in the blood, lymph**
806 **nodes and spleen during ageing.**

807 **a-c**, Representative flow cytometry plots (left) and quantification (right) of the percentage
808 of CD4⁺ cells in the blood (a), lymph nodes (b) and spleen (c) from young (3 mo) and old
809 (24 mo) mice (n = 5-9 mice per group).

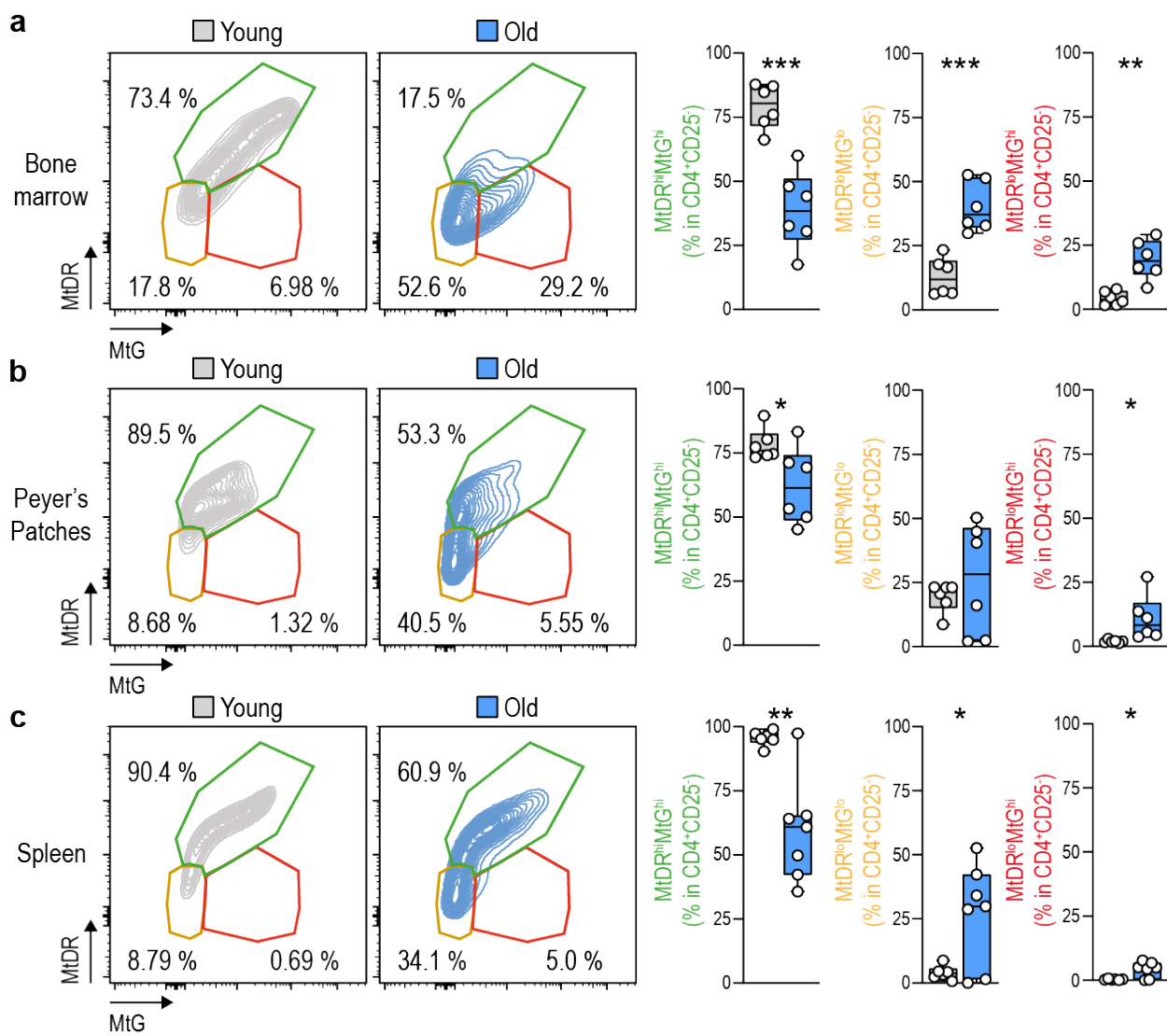
810 **Extended Data Figure 4**



811 **Extended Data Figure 4 | Expression of markers identifying CD4⁺ clusters in the BM.**

812 UMAP representation of the expression levels of markers used to identify the different
813 populations of BM CD4⁺ cells shown in Fig. 2a.

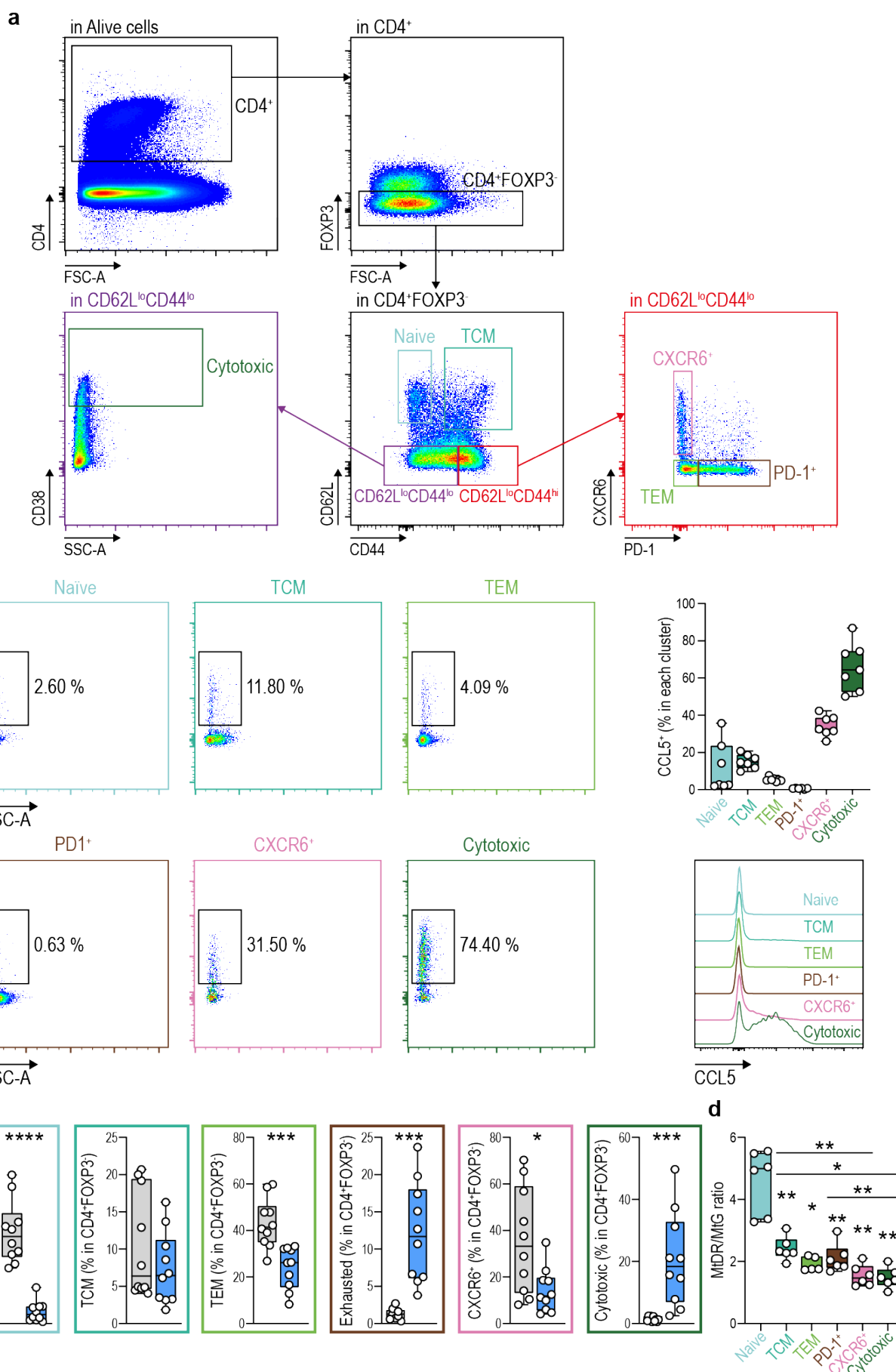
814 **Extended Data Figure 5**



815 **Extended Data Figure 5 | CD4⁺ T cells with dysfunctional mitochondria preferentially
816 accumulate in the BM.**

817 **a-c**, Representative contour plots (right) and quantification of the percentage of CD4⁺
818 cells exhibiting polarized (MtDR^{hi}MtG^{lo}) and depolarized (MtDR^{lo}MtG^{lo} or
819 MtDR^{lo}MtG^{hi}) mitochondria in the BM (a), Peyer's Patches (b) and the spleen (c) from
820 young (3 mo) and old (24 mo) mice (n = 6 mice per group).

821 **Extended Data Figure 6**

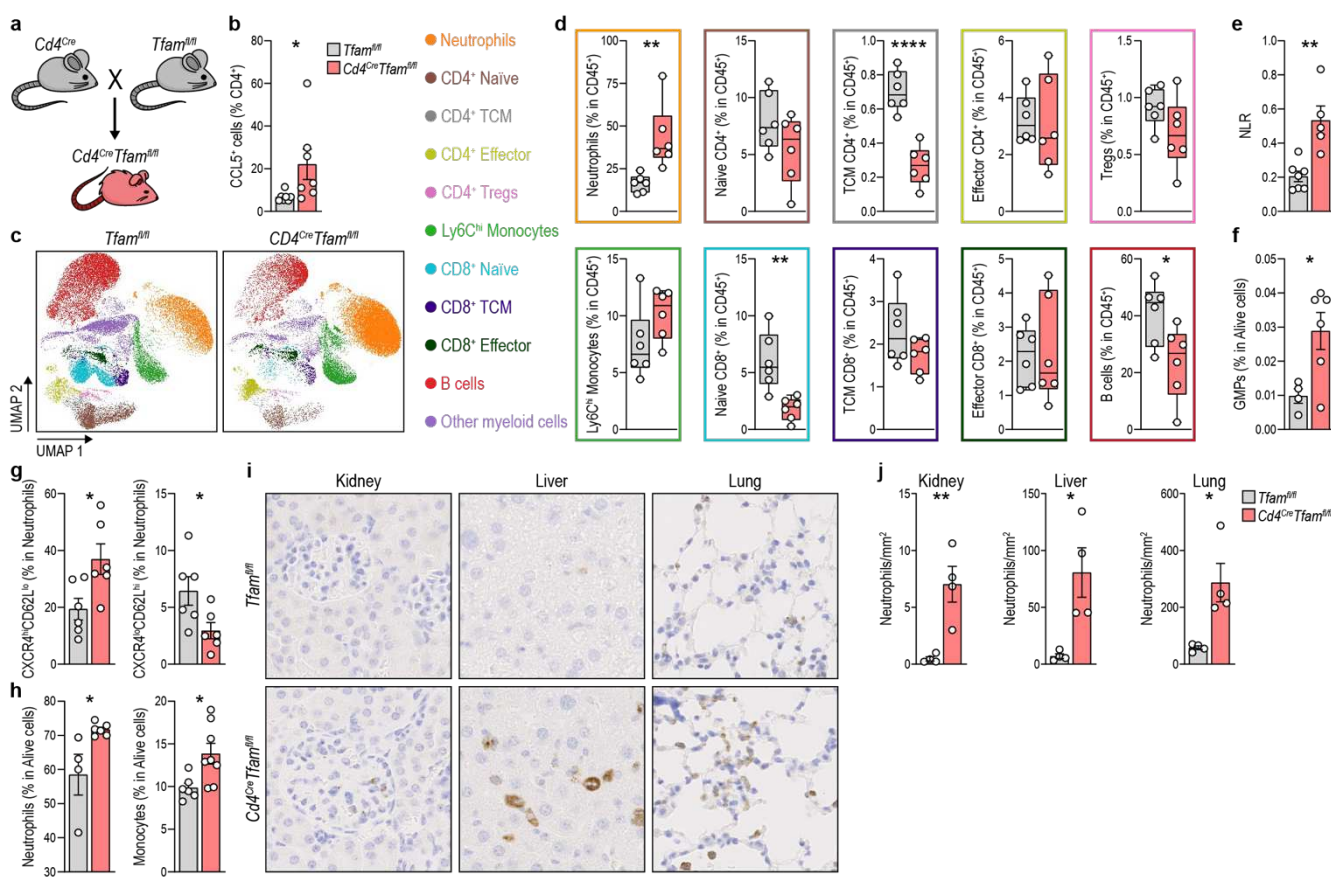


822 **Extended Data Figure 6 | Identification of CD4⁺ CTLs by surface markers.**

823 **a**, Intracellular staining demonstrating the successful identification of all T cell clusters
824 identified in the BM by extracellular staining. T regulatory cells were excluded by gating
825 on CD4⁺Foxp3⁻ cells (for extracellular staining Foxp3 was substituted by CD25). First,
826 Naïve (CD4⁺CD62L^{hi}CD44⁻) and TCM (CD4⁺CD62L^{hi}CD44⁺) cells were identified.
827 Then, CD44^{hi}CD62L⁻ cells or CD44^{lo}CD62L⁻ were gated. CXCR6⁺ (CD4⁺CD62L⁻
828 CD44^{hi}PD-1⁻CXCR6^{hi}), PD-1⁺ (CD4⁺CD62L⁻CD44^{hi}CXCR6⁻PD-1⁺) and TEM
829 (CD4⁺CD62L⁻CD44^{hi}CXCR6⁻PD-1⁻) cells were identified in the CD44^{hi}CD62L⁻
830 population. CD4⁺ CTLs were identified as CD4⁺CD62L⁻CD44^{lo}CD38^{hi}. **b**,
831 Representative flow cytometry staining for CCL5 in all identified clusters. A high
832 enrichment of CCL5⁺ cells is observed in the population corresponding to CD4⁺ CTLs.
833 (**right up**), Boxplots showing the quantification of the percentage of CD4⁺ CCL5⁺ cells
834 included on each cluster when identified by extracellular multiparametric spectral flow
835 cytometry staining in BM samples from old (24 months old, mo) mice (n = 10 mice per
836 group). (**right down**), Representative histogram showing the expression of CCL5 in the
837 different clusters (n = 7 mice per group). **c**, Boxplots showing the quantification of the
838 percentage of each cluster in CD4⁺Foxp3⁻ cells identified by extracellular multiparametric
839 spectral flow cytometry staining in BM samples from young (3 mo) and old (24 mo) mice
840 (n = 10 mice per group). The frequencies and percentages of cells on each cluster are
841 similar to the observed by intracellular staining. **d**, MtDR/MtG geometric mean
842 fluorescence intensity ratio in all identified clusters in BM samples from old mice (n = 6
843 mice per group).

844

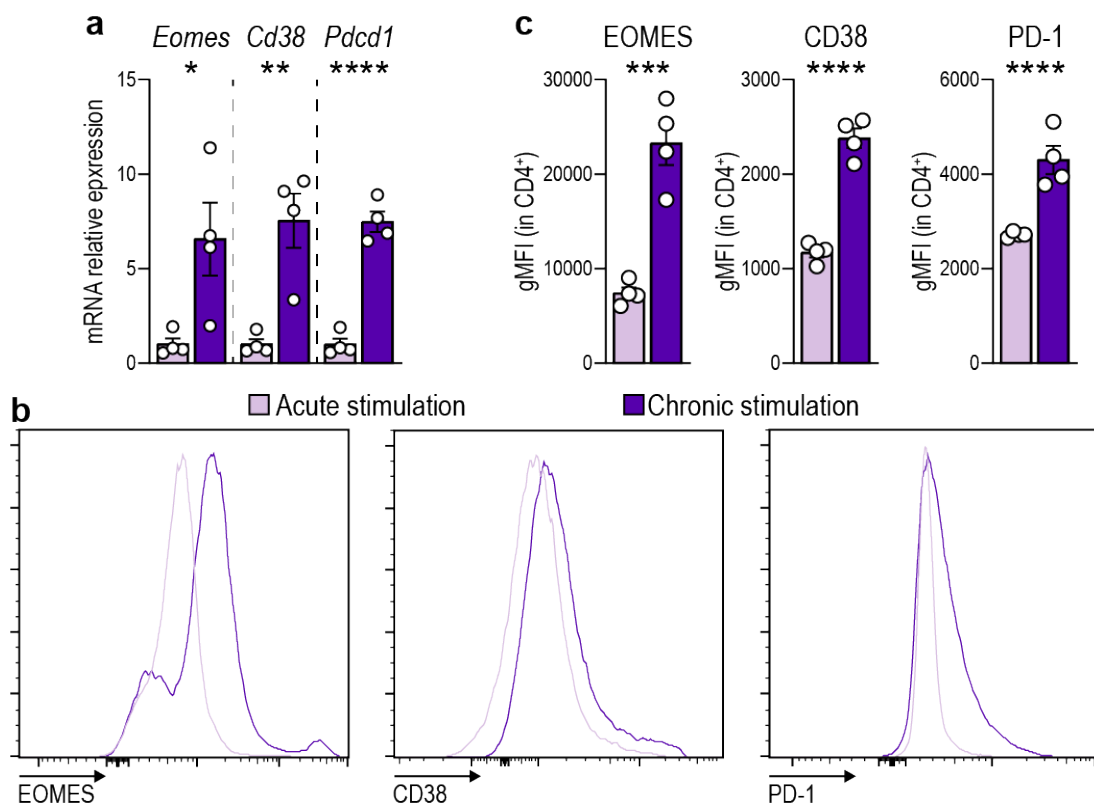
845 **Extended Data Figure 7**



846 **Extended Data Figure 7 | Genetic induction of a mitochondrial dysfunction in T cells enhances granulopoiesis and neutrophil output in mice.**

848 **a**, Diagram showing the genetic strategy followed to generate $CD4^{Cre}$ $Tfam^{fl/fl}$ mice. **b**,
849 Percentage of splenic $CD4^+$ CCL5 $^+$ cells in $Tfam^{fl/fl}$ and $CD4^{Cre}$ $Tfam^{fl/fl}$ mice (n = 7 mice
850 per group). **c**, UMAP with Cluster-X overlay showing the distribution of the eleven
851 clusters of immune cells identified by multiparametric spectral flow cytometry in the
852 circulation of $Tfam^{fl/fl}$ (8 months old, mo) and $CD4^{Cre}$ $Tfam^{fl/fl}$ (8 mo) mice. **d**, Boxplots
853 comparing the percentage of the different depicted populations in $Tfam^{fl/fl}$ and $CD4^{Cre}$
854 $Tfam^{fl/fl}$ mice (n = 6 mice per group). **e**, Quantification of the NLR in the circulation of
855 $Tfam^{fl/fl}$ and $CD4^{Cre}$ $Tfam^{fl/fl}$ mice (n = 5-7 mice per group). **f**, Percentage of GMPs in the
856 BM of $Tfam^{fl/fl}$ and $CD4^{Cre}$ $Tfam^{fl/fl}$ mice (n = 4-6 mice per group). **g**, Quantification of
857 the percentage of CXCR4 hi CD62L lo and CXCR4 lo CD62L hi neutrophils in blood from of
858 $Tfam^{fl/fl}$ and $CD4^{Cre}$ $Tfam^{fl/fl}$ mice (n = 4-6 mice per group). **h**, Percentage of neutrophils
859 and Ly6C hi monocytes in the BM of $Tfam^{fl/fl}$ and $CD4^{Cre}$ $Tfam^{fl/fl}$ mice (n = 4-6 mice per
860 group). **i**, Immunohistochemistry for MPO in kidney, liver and lung sections from $Tfam^{fl/fl}$
861 and $CD4^{Cre}$ $Tfam^{fl/fl}$ mice (n = 4 mice per group). **j**, Quantification of myeloperoxidase-
862 positive neutrophils per area.

863 **Extended Data Figure 8**



864 **Extended Data Figure 8 | Prolonged TCR stimulation induces the expression of**
865 **CD4⁺CTL markers in vitro.**

866 **a-c**, mRNA (**a**) and protein (**b,c**) levels of EOMES, CD38 and PD-1 in T cells acutely or
867 chronically stimulated *in vitro* with anti-CD3/anti-CD28 determined by RT-qPCR
868 analysis and flow cytometry, respectively (n = 4).